NMR Relaxation Order Parameter Analysis of the Dynamics of Protein Side Chains

David M. LeMaster*

Contribution from the Chemical Science and Technology Group 4, Los Alamos National Laboratory, Los Alamos, New Mexico 87545

Received August 19, 1998. Revised Manuscript Received December 9, 1998

Abstract: An arbitrary multiexponential representation of the H−X bond reorientation autocorrelation function is shown to provide robust predictions of both the fast limit (S_f^2) and generalized (S^2) order parameters for macromolecular NMR relaxation analysis. This representation is applied to the analysis of side-chain dynamics in *Escherichia coli* thioredoxin to assess correlated torsional fluctuations and the resultant configurational entropy effects. For both the high S^2 phenylalanine and low S^2 leucine side chains, torsional fluctuations in the major rotamer conformation can predict the observed relaxation data only if main-chain−side-chain torsional correlations are assumed. Crankshaft-like correlations occur around the side-chain χ_2 rotation axis and the parallel main-chain rotation axis. For the sterically hindered buried side chains, torsional fluctuations are predicted to be attenuated for the main-chain rotation axis oriented gauche to the χ_2 rotation axis. Weaker main-chain−side-chain torsional correlations appear to be present for the highly solvated mobile side chains as well. For these residues, the fast limit order parameter is interpretable in terms of fluctuations within a rotamer state, while the decrease in the order parameter due to motion near the Larmor frequencies can be used to estimate the entropy of rotamer exchange.

I. Introduction

As applied to biomacromolecular NMR studies, the heteronuclear T_1, T_2, and NOE relaxation experiments monitor the decay of the autocorrelation function of the H−X dipole (and chemical shift anisotropy) interaction. To date, a large number of ^{15}N as well as a smaller set of ^{13}C C^α relaxation studies have been used to characterize protein main-chain dynamics. Side-chain dynamics studies have primarily focused on techniques for analyzing methyl relaxation,[1−5] although more recently techniques have been introduced for monitoring the side-chain methine and methylene positions as well.[4,6] Unfortunately, the corresponding advance in understanding of the internal molecular dynamics of proteins has been hampered by ambiguities as to the optimal means of interpreting the experimental relaxation data. The widely used "model-free" dynamical formalism of Lipari and Szabo[7] interprets macromolecular internal dynamics in terms of a generalized order parameter, S^2, and an effective time constant of motion, τ_e, derived from a single-exponential representation of the internal autocorrelation function. The generalized order parameter S^2 characterizes the degree to which information on the orientation of an individual H−X bond vector is lost due to dynamical processes. More specifically, S^2 represents the component of the H−X bond vector autocorrelation function which is dissipated by global molecular tumbling, while $(1 - S^2)$ characterizes the bond vector orientational disorder arising from internal motion occurring more rapidly than the molecular tumbling.

Unfortunately, the two-parameter Lipari−Szabo formalism is unable to adequately fit the experimental data for a significant fraction of the observed protein relaxation data. This effect is most marked in the case of side-chain dynamics. For example, only 12% of all side-chain aliphatic methine and methylene T_1, T_2, and NOE relaxation data of *Escherichia coli* thioredoxin[4] can be fitted by the (S^2,τ_e) formalism with χ^2 probabilities above 0.05. Three-parameter extensions of the Lipari−Szabo formalism have been introduced so as to accommodate relaxation data which reflect more extensive motion occurring near the Larmor frequencies.[8,9] In these three-parameter dynamical formalisms, there is a 1-to-1 mapping between the dynamical variables and the T_1, T_2, and NOE relaxation values over a wide range of experimental data.[9] Hence, the ability to fit given experimental relaxation data does not provide a particularly stringent test for the validity of the assumptions underlying the dynamical formalism. Due to such considerations, the physical significance of the dynamical parameters derived from experimental data via the Lipari−Szabo type formalisms has been called into question.[10,11]

In principle, the order parameter representation underlying the Lipari−Szabo type formalisms provides a direct physical interpretation of dynamics, as the S^2 values are directly related to the variance of the probability-weighted spherical harmonics,

* Phone: (505) 667-6686. Fax: (505) 667-0110. E-mail: lemaster@lanl.gov.

(1) Nicholson, L. K.; Kay, L. E.; Baldisseri, D. M.; Arango, J.; Young, P. E.; Bax, A.; Torchia, D. A. *Biochemistry* **1992**, *31*, 5253.
(2) Palmer, A. G.; Hochstrasser, R. A.; Millar, D. P.; Rance, M.; Wright, P. E. *J. Am. Chem. Soc.* **1993**, *115*, 6333.
(3) Muhandiram, D. R.; Yamazaki, T.; Sykes, B. D.; Kay, L. E. *J. Am. Chem. Soc.* **1995**, *117*, 11536.
(4) LeMaster, D. M.; Kushlan, D. M. *J. Am. Chem. Soc.* **1996**, *118*, 9255.
(5) Lee, A. L.; Urbauer, J. L.; Wand, A. J. *J. Biomol. NMR* **1997**, *9*, 437.
(6) Yang, D.; Mittermaier, A.; Mok, Y. K.; Kay, L. E. *J. Mol. Biol.* **1998**, *276*, 939.
(7) Lipari, G.; Szabo, A. *J. Am. Chem. Soc.* **1982**, *104*, 4546.
(8) Clore, G. M.; Szabo, A.; Bax, A.; Kay, L. E.; Driscoll, P. C.; Gronenborn, A. M. *J. Am. Chem. Soc.* **1990**, *112*, 4989.
(9) LeMaster, D. M. *J. Biomol. NMR* **1995**, *6*, 366.
(10) Peng, J. W.; Wagner, G. *Biochemistry* **1992**, *31*, 8571.
(11) Ishima, R.; Yamasaki, K.; Nagayama, K. *J. Biomol. NMR* **1995**, *6*, 423.

10.1021/ja982988r CCC: $18.00
Published on Web 02/02/1999

σ^2_{Y2m}, which characterizes the orientational disorder of the H−X bond vector.[12]

$$S^2 = 1 - \frac{4\pi}{5}\sum_{m=-2}^{2}\sigma^2_{Y2m} \quad (1)$$

In section II, it is demonstrated that robust estimates of both the fast limit S_f^2 and generalized S^2 order parameters can be derived for any dynamical process in which the corresponding autocorrelation function can be represented as an arbitrary multiexponential expansion. As further discussed in that section, such dynamical representations include the widely observed log-normal and $1/f$ distributions which arise from random multiplicative processes.[13−15] Energy landscape analyses ranging from glass flow dynamics[16] to protein folding[17] fall within this class of dynamical processes. The multiexponential representation analysis provides for quantitative partitioning of the order parameter contributions of dynamical processes with time constants shorter than ∼50 ps from those of slower processes with time constants up to that of the global tumbling of the macromolecule.

In section III, the experimental fast limit order parameter data obtained for *E. coli* thioredoxin is used to interpret protein side-chain relaxation in terms of dynamical processes which can be characterized by fluctuations within a localized potential minimum. Central to this analysis is explicit consideration of correlated torsional fluctuations.

One view of the basis for the high cooperativity observed in protein unfolding is that the protein expansion must achieve a certain threshold to provide the entropic benefit of freeing the rotation of the buried side chains.[18] Clearly, experimental determination of individual side-chain entropies would provide a quantitative assessment of this contribution to overall protein stability as well as for a wide range of protein−ligand interactions. It has been proposed that order parameters can be interpreted in terms of local configurational entropy.[19] Such entropy analyses have generally invoked the assumption of independent bond vector fluctuations.[19−23] The assumption of independent bond vector fluctuations has generally reflected the fact that the available experimental relaxation data have sampled only a limited set of atomic positions, most commonly either main-chain ^{15}N resonances or ^{13}C methyl resonances, so that a more realistic dynamical representation cannot be adequately experimentally constrained.

However, various lines of evidence argue against the general validity of the assumption of independent bond vector fluctuations for configurational entropy analysis. Particularly germane to the present analysis, protein leucine methyl relaxation studies[3,4,24] have noted that, for many residues, the order parameters of the geminal methyl rotation axes are not equivalent which appears to contradict the assumption of a direct correspondence between order parameter and local configurational entropy. Also pertinent is the fact that the C^β positions of half of the aromatic residues of *E. coli* thioredoxin have order parameters lower than those of either the C^α or ring carbons, strongly suggestive of correlated motion.[4]

Proper accounting for the presence of correlated motion avoids the systematic overestimate of configurational entropy which results from the assumption of independent bond vector fluctuations. Experimental assessment of correlated motion is particularly of value, as configurational entropy estimates based on molecular simulations have proven problematic due to uncertainities regarding how completely the accessible configurational space is sampled.[25]

Using the extensive ^{13}C and ^{15}N relaxation data available for *E. coli* thioredoxin, it is demonstrated in section III that the entropic contribution of correlated side-chain motion can be realistically estimated from experimental data. Dynamical analysis of the large buried side chains in *E. coli* thioredoxin, for which only fast limit motion contributes to the internal ^{1}H−^{13}C bond autocorrelation function, indicates that main-chain−side-chain torsional fluctuations in the major rotamer state must be correlated in order to accommodate the observed relaxation data. Application of this correlation analysis to leucine side-chain dynamics is particularly germane, as the low order parameters observed for the methyl rotation axes of these residues have previously been interpreted in terms of large-scale internal motions.[1,24]

In section IV, attention is turned to the physical interpretation of the decay of the order parameter which occurs in the time frame bounded by the fast limit processes and the overall macromolecular tumbling. In section IVA, side-chain rotamer exchange entropies are shown to be experimentally accessible from relaxation measurements, even in the absence of independent estimates of the populations of the individual rotameric states. In section IVB, this analysis is applied to the dynamics of the highly solvated surface side chains of *E. coli* thioredoxin. Combined analysis of the main-chain and side-chain dynamics for these comparatively unhindered side chains indicates that, in these cases, the fast limit and generalized order parameters can be reliably interpreted in terms of fluctuations within a rotamer state and exchange between rotamer states, respectively. Furthermore, even in the case of these relatively unhindered side chains, the assumption of uncorrelated main-chain−side-chain motion appears to be unjustified.

IIA. Experimental Analysis of the Range of Applicability of the Lipari−Szabo Formalism for Protein Side-Chain Dynamics

In the second of their classic papers, Lipari and Szabo provide estimates of the range of applicability for their model-free dynamical formalism.[26] If the molecular tumbling time τ_M is at least 100-fold longer than the effective internal correlation time τ_e and the time constant for the highest sampled Larmor frequency (i.e., $1/\omega_{H+C}$) is at least 10-fold longer than τ_e, then τ_e and S^2 values accurate to a few percent can be extracted from either T_1 and NOE values at one field or T_1 values at two fields. Note that these conditions correspond to $\tau_e < 25$ ps at currently typical magnetic fields. In practice, the (S^2,τ_e) formalism has routinely been applied far beyond that proposed range of applicability. For cases in which three or more independent

(12) Bruschweiler, R.; Wright, P. E. *J. Am. Chem. Soc.* **1994**, *116*, 8426.
(13) Montroll, E. W.; Shlesinger, M. F. *Proc. Natl. Acad. Sci. U.S.A.* **1982**, *79*, 3380.
(14) Stanley, H. E.; Meakin, P. *Nature* **1988**, *335*, 405.
(15) Weissman, M. B. *Rev. Mod. Phys.* **1988**, *60*, 537.
(16) Littau, K. A.; Dugan, M. A.; Chen, S.; Fayer, M. D. *J. Chem. Phys.* **1992**, *96*, 3484.
(17) Bryngelson, J. D.; Wolynes, P. G. *J. Phys. Chem.* **1989**, *93*, 6902.
(18) Shaknovich, E. I.; Finkelstein, A. V. *Biopolymers* **1989**, *28*, 1667.
(19) Akke, M.; Bruschweiler, R.; A. G. Palmer, I. *J. Am. Chem. Soc.* **1993**, *115*, 9832.
(20) Yang, D.; Kay, L. E. *J. Mol. Biol.* **1996**, *263*, 369.
(21) Li, Z.; Raychaudhuri, S.; Wand, A. *J. Protein Sci.* **1996**, *5*, 2647.
(22) Yang, D.; Mok, Y. K.; Forman-Kay, J. D.; Farrow, N. A.; Kay, L. E. *J. Mol. Biol.* **1997**, *272*, 790.
(23) Gagne, S. M.; Tsuda, S.; Spyracopoulos, L.; Kay, L. E.; Sykes, B. D. *J. Mol. Biol.* **1998**, *278*, 667.
(24) Wand, A. J.; Urbauer, J. L.; McEvoy, R. P.; Bieber, R. J. *Biochemistry* **1996**, *35*, 6116.
(25) Edholm, O.; Berendsen, H. J. C. *Mol. Phys.* **1984**, *51*, 1011.
(26) Lipari, G.; Szabo, A. *J. Am. Chem. Soc.* **1982**, *104*, 4559.

experimental relaxation constraints are available, a necessary condition for the applicability of this two-parameter formalism is the ability to fit the experimental data to within experimental uncertainty. Indeed, the inability of the (S^2,τ_e) formalism to fit a significant fraction of the ^{15}N relaxation data of interleukin 1β led Clore, Szabo, and co-workers to propose an extended three-parameter dynamical formalism.[8]

Although more extensive dynamical heterogeneity can be anticipated for the protein side chains, simple two-parameter dynamical formalisms have been invoked in several recent studies.[6,22,27,28] This choice has primarily reflected the fact that the side-chain relaxation experiments utilizing uniform ^{13}C-enriched samples proposed to date have been limited to two of the three standard T_1, T_2, and NOE autocorrelation experiments. One-bond ^{13}C homonuclear scalar and dipolar couplings severely complicate ^{13}C relaxation experiments in uniform ^{13}C-labeled samples.[29] Furthermore, dynamical interpretation of relaxation decay curves for methyl and methylene positions are complicated by ^{1}H$-^{13}$C dipole cross correlation,[30,31] although pulse sequences designed to suppress these effects for methyl groups have been introduced.[1,32] Based on analysis assuming Lipari−Szabo dynamics, it has been argued that ^{1}H$-^{13}$C dipole cross correlation yields only modest errors in ^{13}C T_1 and NOE experiments.[33] This assumption has recently been invoked in the ^{13}C side-chain relaxation analysis of RNase T_1.[28]

To circumvent the complications of the ^{13}C homonuclear scalar and dipolar interactions as well as those of ^{1}H$-^{13}$C cross correlation, Kay and co-workers[3,6] have introduced a set of ^{2}H relaxation experiments applicable to random fractionally deuterated uniform ^{13}C-enriched samples for which cross correlation and cross relaxation effects are minimal.[34] Unfortunately, as only T_1 and $T_{1\rho}$ experiments are applicable, sampling of the higher frequencies offered by the ^{13}C NOE experiment is lost.

Selective ^{13}C enrichment combined with random fractional ^{2}H enrichment and IS spin selection provides a means of obtaining ^{13}C T_1, T_2, and NOE data at most side-chain positions free of the complications referred to above.[4] Analysis of the ability of the (S^2,τ_e) formalism to simultaneously fit these experimental data can serve to determine the outer bounds for which the two-parameter Lipari−Szabo formalism is applicable to protein side-chain dynamics. Such an analysis using the ^{13}C relaxation data of *E. coli* thioredoxin is simplified by the marked constancy of the ^{15}N and C$^\alpha$ T_1 and T_2 values for the great majority of the residues in this proteins,[4,35] strongly indicative of isotropic tumbling consistent with the approximately spherical X-ray structure.[36]

Optimal fits of S^2 and τ_e for 135 side-chain methine and methylene resonances of *E. coli* thioredoxin were obtained using the experimental uncertainties for reported T_1, T_2, and NOE values (median experimental uncertainty ~3%).[4] In panel A of Figure 1 are illustrated the individual χ^2 probabilities greater than (●) or less than (×) 0.05 as a function of the experimental NOE and normalized T_1/T_2 values. For nuclei exhibiting only fast limit internal motion, both T_1/T_2 and NOE values are independent of S^2 and depend dynamically only on the molecular tumbling time. The data for such nuclei lie near the apex of the apparent triangle (i.e., normalized $T_1/T_2 \approx 1$ and NOE ≈1.2),

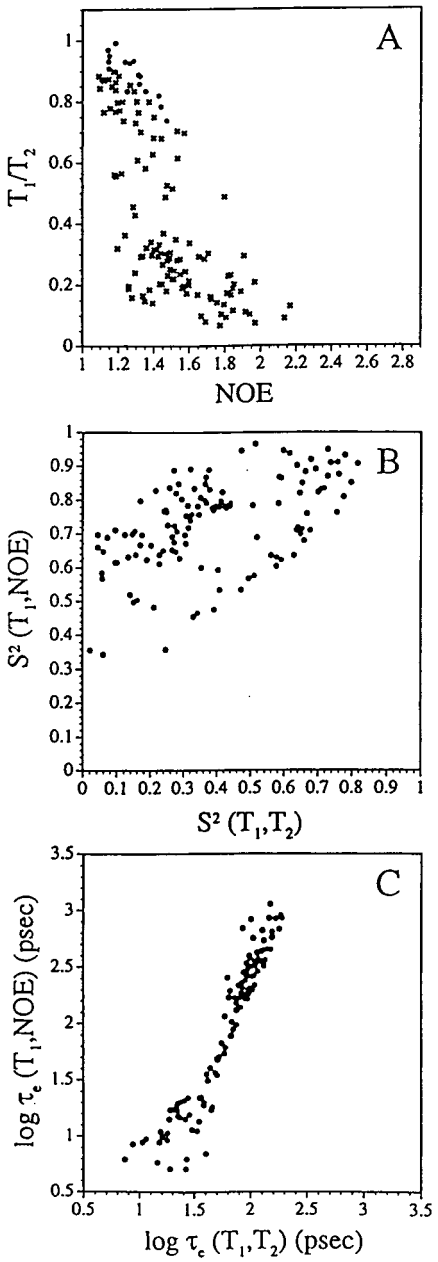

Figure 1. Dynamical analysis of the ^{13}C T_1, T_2, and NOE values from 135 side-chain aliphatic methine and methylene positions of *E. coli* thioredoxin according to the (S^2,τ_e) Lipari−Szabo formalism. Positions exhibiting apparent chemical exchange broadening[4] have been removed, as have four positions exhibiting NOE values more than 2σ below the rigid tumbling limit value. The optimal fits were obtained via a grid search over S^2 with a grid spacing of 0.002 and log τ_e with a grid spacing of 0.007. Assuming one degree of freedom, the χ^2 probabilities greater than (●) and less than (×) 0.05 are plotted in panel A as a function of T_1/T_2 and NOE. The experimental T_1/T_2 values have been normalized to the rigid tumbling limit value. The previously reported experimental uncertainties and global correlation times were assumed.[4] Panels B and C illustrate the S^2 and log τ_e values estimated from the same experimental data by applying the Lipari−Szabo dynamical formalism to only the (T_1,NOE) and the (T_1,T_2) data.

(27) Constantine, K. L.; Friedrichs, M. S.; Wittekind, M.; Jamil, H.; Chu, C. H.; Parker, R. A.; Goldfarb, V.; Mueller, L.; B. T. Farmer, I. *Biochemistry* **1998**, *37*, 7965.
(28) Engelke, J.; Ruterjans, H. *J. Biomol. NMR* **1998**, *11*, 165.
(29) Yamazaki, T.; Muhandiram, R.; Kay, L. E. *J. Am. Chem. Soc.* **1994**, *116*, 8266.
(30) Fagerness, P. E.; Grant, D. M.; Kuhlmann, K. F.; Mayne, C. L.; Parry, R. B. *J. Chem. Phys.* **1975**, *63*, 2524.
(31) Vold, R. R.; Vold, R. L. *J. Chem. Phys.* **1976**, *64*, 320.
(32) Palmer, A. G.; Wright, P. E.; Rance, M. *Chem. Phys. Lett.* **1991**, *185*, 41.
(33) Zhu, L.; Kemple, M. D.; Landy, S. B.; Buckley, P. *J. Magn. Reson.* **1995**, *109*, 19.
(34) Yang, D.; Kay, L. E. *J. Magn. Reson. B* **1996**, *110*, 213.
(35) Stone, M. J.; Chandrasekhar, K.; Holmgren, A.; Wright, P. E.; Dyson, H. J. *Biochemistry* **1993**, *32*, 426.
(36) Katti, S.; LeMaster, D. M.; Eklund, H. *J. Mol. Biol.* **1990**, *212*, 167.

and as expected all are well fitted by the (S^2,τ_e) formalism. The downward deviation of the T_1/T_2 and NOE values from the apex of this triangle provides a qualitative measure of the magnitude and effective time frame of the internal motion occurring in the approximately nanosecond range.[9] The other relaxation data predicting χ^2 probabilities above 0.05 lie along the upper right boundary of the apparent triangle, consistent with effective time constants near the fast limit. The vast majority of the dynamical range is filled by relaxation data which is incompatible with the two-parameter formalism.

Hence, when data from all three standard autocorrelation relaxation experiments are available, the appropriate dynamical range for the Lipari−Szabo formalism can be directly assessed by the parameter fit relative to the experimental uncertainties. The situation is far less transparent when only two of the three relaxation data sets are available. Nearly all of the experimental data of Figure 1A can be perfectly fitted with (S^2,τ_e) parameters using only the (T_1,NOE) or (T_1,T_2) data. In panel B of Figure 1 are illustrated the S^2 values estimated for the experimental data of panel A using only the (T_1,NOE) and the (T_1,T_2) data. The correlation between the two estimates of S^2 is virtually nonexistent. The only unambiguous result is that S^2 estimates based on the (T_1,NOE) data are systematically higher than those derived from the (T_1,T_2) data.

The S^2 values derived from the (T_1,T_2) data agree quite well with those obtained from the multiexponential autocorrelation function analysis discussed in the following section, with no discrepancies larger than 0.05, and the vast majority of estimates within 0.02. These robust estimates of S^2 hold for relaxation data lying far outside the Lipari−Szabo regime. As we have previously shown,[9] the generalized order parameter is quite reliably determined directly from T_1 and T_2 data without recourse to modeling of the internal autocorrelation function.

$$S^2 = (1/T_2 - 1/T_1)/(1/T_{2R} - 1/T_{1R}) \qquad (2)$$

where R denotes the rigid tumbling limit value. For macromolecules tumbling appreciably slower than the heteronuclear Larmor frequency, this estimate of the generalized order parameter is expected to hold for all internal motion which has rates comparable to or faster than the heteronuclear Larmor frequency.

Clearly, in general the S^2 values obtained using only (T_1, NOE) data to fit the Lipari−Szabo formalism are unreliable for globular macromolecules. A more conservative application would be to only consider S^2 values based on (T_1,NOE) data for which the predicted τ_e value is less than 25 ps in hopes of empirically estimating the dynamical bounds for the Lipari−Szabo formalism. When compared against the corresponding S^2 values obtained from only (T_1,T_2) data (which are highly reliable in this dynamical regime), the ΔS^2 values range from 0.004 to 0.242, with 15% being in excess of 0.2. Arguments that T_1 values alone can be used to derive S^2 values[37] have assumed Lipari−Szabo dynamics and appear to be of little practical significance for macromolecular analysis. Not only is the argument invalid outside of the Lipari−Szabo regime, but also T_1 and NOE data appear to be insufficient to establish whether Lipari−Szabo dynamics apply.

In panel C of Figure 1 is illustrated the corresponding comparison of τ_e values estimated from the experimental data of panel A using either (T_1,NOE) or (T_1,T_2) data. Two distinct regions are apparent. In the nominal Lipari−Szabo range below ~30 ps (i.e., log τ_e = 1.5), the τ_e values estimated from the (T_1, NOE) and (T_1,T_2) data are again largely uncorrelated. The τ_e values obtained from the (T_1,T_2) data are systematically longer than those estimated from (T_1,NOE) data. Above 30 ps, the predicted τ_e values obtained from the (T_1,NOE) and (T_1,T_2) data are much more strongly correlated, with a slope significantly higher than the expected value of 1.0. As discussed in more detail in the following section, estimation of an effective time constant in this dynamic regime is problematic, even when all three autocorrelation relaxation values are known. However, the time constants estimated from the (S^2,τ_e) fit to the (T_1,NOE) and (T_1,T_2) data are dramatically smaller than the corresponding dominant time constants estimated from the multiexponential autocorrelation function analysis of the complete T_1, T_2, and NOE data. In particular, the τ_e values obtained from the (T_1,T_2) data are on average 9-fold smaller, with a substantial dispersion in the individual ratios.

In summary, for the situation in which only experimental T_1 and NOE data are available, it is unclear whether any quantitative assessment of macromolecular dynamics can be validly drawn. In the absence of an effective monitor of the $J(0)$ contribution to the spectral density function, normally provided by T_2 measurements, separation of the contributions from internal motion vs global tumbling is problematic. The situation is more favorable in the case of the T_1 and $T_{1\rho}$ (or T_2) data sets as obtained from the ^{2}H relaxation experiments developed by Kay and co-workers.[3] In this case, robust estimates of S^2 can be obtained which appear to become only modestly unreliable when substantial internal orientational disorder occurs at a rate comparable to the heteronuclear Larmor frequency. On the other hand, effective time constants derived from analysis of only T_1 and T_2 data can only be considered highly qualitative at best.

The standard T_1, T_2, and NOE autocorrelation experiments can potentially be augmented by cross correlation experiments such as the dipolar cross-correlated cross relaxation (SIIS) experiment introduced by Ernst and Ernst.[38] This experiment samples the spectral density function at zero frequency and at the ^{13}C Larmor frequency, which in turn are the terms which generally dominate macromolecular T_1 and T_2 (or $T_{1\rho}$) values. Using both ^{2}H autocorrelation and ^{13}C cross correlation measurements on a labeled SH3 domain, Kay and co-workers have demonstrated that the SIIS cross-correlated cross relaxation rates are approximately proportional to the ^{2}H−^{13}C bond generalized order parameters.[6] Since the SIIS cross-correlated cross relaxation rate is directly related to the S_{HCH}^2 order parameter, it provides an additional constraint on the possible motions consistent with the generalized order parameter S^2. However, these cross correlation data can provide little additional information regarding either the time frame of this internal motion or the partitioning of motion between fast limit and slower motions.

IIB. Multiexponential Expansion of the Internal Autocorrelation Function

The generalized order parameter S^2 characterizes the fraction of the autocorrelation function which is quenched by the global molecular tumbling. Internal motions slower than molecular tumbling influence the observed relaxation values only via the T_2 effects of chemical exchange arising from motion in the micro- to millisecond regime. Field strength dependence[39] and

(37) Fushman, D.; Weisemann, R.; Thuring, H.; Ruterjans, H. *J. Biomol. NMR* **1994**, *4*, 61.

(38) Ernst, M.; Ernst, R. R. *J. Magn. Reson. Ser. A* **1994**, *110*, 202.

(39) Gutowsky, H. S.; Holm, C. H. *J. Chem. Phys.* **1956**, *23*, 1228.

spin-lock[40,41] studies can be used to deconvolute the chemical exchange contribution, as will be assumed in the following analysis. The correlation function describing diffusive isotropic molecular tumbling is given by

$$C_o(t) = {}^1/_5 e^{-1/\tau_M} \quad (3)$$

where τ_M is the global tumbling time. The autocorrelation functions and resultant spectral density functions for both symmetric and asymmetric ellipsoidal diffusion tensors have been described.[7,42] Proteins exhibiting symmetric[43] and asymmetric[44] ellipsoidal diffusion have been characterized. For the isotropic case, if the overall and internal motions are independent, the total correlation function can be rigorously factored. Model calculations indicate that an analogous separability of internal and overall motion is operationally valid for modestly anisotropic ellipsoidal diffusion, consistent with the relaxation analysis of native globular proteins.[44,45]

If, in addition to separability, the internal correlation function can be represented as a sum of exponentials,

$$C_i(t) = S^2 + \sum \alpha_i e^{-1/\tau_i'} \quad (4)$$

the total correlation function can then be represented as

$$C(t) = {}^1/_5 S^2 e^{-1/\tau_M} + {}^1/_5 \sum \alpha_i e^{-1/\tau_i} \quad (5)$$

where the time constants $1/\tau_i = 1/\tau_M + 1/\tau_i'$, with τ_i' denoting the time constants of the internal autocorrelation function and the sum of the amplitudes α_i equaling $1 - S^2$. In this case, S^2 represents the limiting value of the internal correlation function for time constants less than τ_M which, as noted by Lipari and Szabo, is experimentally indistinguishable from the infinite time limit order parameter.[7]

Reliable decomposition of experimental data into a sum of exponentials containing similar time constants is notoriously problematic unless the (small) number of terms is known a priori.[46] Given a maximum of five data points (i.e., the experimentally sampled spectral density values), such an approach is fruitless for analyzing relaxation data. A differing approach can be taken by noting that relaxation effects arise from three distinct frequency regimes. Motions having characteristic frequencies significantly above the highest spectral density component sampled in the relaxation experiment (i.e., ω_{H+C} for ^{13}C relaxation) attenuate the relaxation interactions without a discernible frequency dependence. Molecular dynamics simulations indicate that librational relaxation in the (sub)-picosecond time frame will lead to a minimum of ~10% decay of the autocorrelation function in the fast limit frequency range.[47] At the other extreme is the previously mentioned relaxation resulting from overall molecular tumbling. The remainder of the relaxation arises from internal motions with characteristic frequencies around the ^1H and heteronuclear Larmor frequencies which differentially affect the various spectral density components monitored by the relaxation experiment, thus giving rise to a discernible frequency dependence.

Following this approach to frequency partitioning, the relevant components of an arbitrary exponential expansion for the internal correlation function can be represented by

$$C_i(t) = \sum_{t=0}^{1/a\omega_{H+C}} \alpha_i e^{-1/\tau_i} + \sum_{t=1/a\omega_{H+C}}^{1/b\omega_C} \beta_i e^{-1/\tau_i} + \sum_{t=1/b\omega_C}^{\tau_M} \gamma_i e^{-1/\tau_i} \quad (6)$$

The potential utility of this frequency partitioning depends on two considerations. It must be possible for every set of experimental (T_1,T_2,NOE) values to define a common scale factor a such that the fast limit orientational disorder represented by the first term of eq 6 is approximately constant, independent of the exponential parameters used to represent the second and third terms of that equation. Furthermore, the scale factor b should be as small as is consistent with an approximately constant estimate of the generalized order parameter S^2. As is apparent from eq 5, a lower limit to the value of b is imposed by the fact that, when internal motions contribute at frequencies near that of the overall tumbling rate, unambiguous separation between internal and overall motion is no longer possible. For the frequency range in which separation into internal and overall motion is ambiguous (i.e., the third term of eq 6), all contributions will be folded into the S^2 value, with the recognition that $b\omega_C$ represents the slowest internal motion monitored. Under these conditions, the spectral density function can be represented as

$$J(\omega) = {}^2/_5 [S^2 \tau_M/(1 + (\omega\tau_M)^2) + \sum_{1/a\omega_{H+C}}^{1/b\omega_C} \beta_i \tau_i/(1 + (\omega\tau_i)^2)] \quad (7)$$

The amplitude of the intermediate frequency motion $\sum\beta_i$ is then identified with the decrease in the order parameter value $S_f^2 - S^2$, which arises from these motions. In principle, the number of Lorentzian terms (N) representing the intermediate frequency internal motion can be arbitrary. However, as determined by the Monte Carlo simulations described below, the resulting mean and standard deviation estimates for S^2 and S_f^2 are essentially invariant for $N > 4$. This upper limit of four Lorentzian terms is a manifestation of the relatively narrow frequency window (ω_{H+C} to ω_C) sampled by the nonzero spectral density components.

Since the sum of the amplitudes in eq 7 is normalized, there are three independent dynamical parameters for the $N = 1$ case, which corresponds closely to the previously proposed extended model-free formalism.[8] As there is a 1-to-1 mapping onto the experimental T_1, T_2, and NOE values for the full range of $N = 1$ dynamical parameters,[9] unique predictions of S^2 and S_f^2 values is trivially valid. It is less transparent as to whether the nine independent dynamical parameters of the $N = 4$ case will map onto the three experimental relaxation values so as to generate an effective constancy in the predicted S^2 and S_f^2 values. As illustrated in section IIC below, using experimental relaxation data from *E. coli* thioredoxin, it is demonstrated that the predicted S^2 and S_f^2 values are largely invariant, regardless of the number of exponential terms used to model the underlying dynamical processes.

It should be noted that eq 7 with $N = 1$ is not strictly equivalent to the (S_f^2,S_s^2,τ_e) representation of the earlier extended model-free formalism.[8] In that earlier derivation, it was argued that, if the fast limit motions are axially symmetric and dynamically independent of the slower internal motions, then

(40) Szyperski, T.; Luginbuhl, P.; Otting, G.; Guntert, P.; Wuthrich, K. *J. Biomol. NMR* **1993**, *3*, 151.
(41) Akke, M.; Palmer, A. G. *J. Am. Chem. Soc.* **1996**, *118*, 911.
(42) Woessner, D. T. *J. Chem. Phys.* **1962**, *37*, 647.
(43) Tjandra, N.; Feller, S. E.; Pastor, R. W.; Bax, A. *J. Am. Chem. Soc.* **1995**, *117*, 12562.
(44) Tjandra, N.; Wingfield, P.; Stahl, S.; Bax, A. *J. Biomol. NMR* **1996**, *8*, 273.
(45) Schurr, J. M.; Babcock, H. P.; Fujimoto, B. S. *J. Magn. Reson. Ser. B* **1994**, *105*, 211.
(46) Lanczos, C. *Applied Analysis*; Prentice Hall, Inc.: Englewood Cliffs, NJ, 1956.
(47) Levy, R. M.; Karplus, M.; McCammon, J. A. *J. Am. Chem. Soc.* **1981**, *103*, 994.

$S^2 = S_f^2 S_s^2$. In the formulation described herein, no such assumption of axial symmetry or independence of time scales is invoked. Conversely, in the present formulation, the amplitude of the intermediate frequency internal motion cannot be simply identified as S^2/S_f^2.

The utility of the present approach derives from the range of internal dynamics for which the corresponding autocorrelation function can be represented as a (potentially continuous) sum of exponentials. As an isolated random process has a correlation function $e^{-t/\tau}$, the correlation function for the sum of such random processes will be trivially represented by a multiexponential expansion. More physically interesting are the autocorrelation functions for familar explicit models, such as restricted diffusion around a fixed axis[48−50] and diffusion in a cone,[51,52] which are expressed as an infinite sum of exponentials. These examples highlight the point that, in general, there can be no expectation of establishing a direct correlation between each exponential time constant component and a specific physical transition. In the present analysis, the time constants serve to assign the corresponding amplitude to specific characteristic frequency ranges of the autocorrelation function.

In an explicit approach to characterizing polymer and protein dynamics, the Smoluchowski equation models the time evolution of the distribution function for the dipole orientation within the time regime in which friction and diffusion prevail over inertial effects, estimated to correspond to time constants greater than 10 ps.[53] Multiexponential solutions to the one-dimensional equation have been derived, and extension to the three-dimensional equation has been explicitly anticipated.[54,55]

Most generally germane is the fact that random multiplicative processes for which the completion of the primary process depends on the previous completion of a set of subprocesses give rise to multiexponential distribution functions.[14] In the simplest analysis, the probability for the primary process P equals the product of the probabilities of the subprocesses $\prod p_i$. When the individual distributions of the log p_i values satisfy the conditions of the central limit theorem, the probability distribution function of P is log-normal. With a sufficiently large variance of the log p_i values, the log-normal distribution approximates an inverse frequency distribution (i.e., scale invariant distribution function of relaxation times $[\rho(\tau)\, d\tau = d\tau/\tau]$) over any finite positive interval.[13] In turn, the $1/f$ distribution implies a $1/f$ "noise" energy fluctuation spectrum.[56]

$1/f$ noise as well as log-normal and $1/f$ distributions are widely observed in solid-state physics.[15] Illustrations most relevant to the current discussion include the demonstration that glass flow dynamics monitored by optical hole burning follows a $1/f$ distribution with a log-normal tail over a time range of 10^{16}.[16] Concepts of energetic "frustration" and roughness of the potential energy surface drawn from analysis of spin glass physics have stimulated the energy landscape view of protein dynamics.[57−59] For the ligand recombination kinetics of myoglobin covering up to a 10^7-fold range in time, both exponential (four-term expansion) and power law expressions could be fitted to the data within experimental error.[60] Interpreting protein folding dynamics using a random energy model with a funnel yields a log-normal distribution of rates.[17] Explanation of $1/f$ noise as manifesting a multiple-relaxation process arising from the roughness of the potential energy surface gains support from the observation of such a frequency dependence in the energy fluctuations in molecular dynamics simulations of water[61] and, more recently, of a polyalanine helix−coil transition.[62]

IIC. Analysis of Experimental Relaxation Data Using a Multiexponential Expansion of the Internal Autocorrelation Function

As a sampling of the physically plausible range of relaxation data, T_1, T_2, and NOE values for 201 side-chain and main-chain aliphatic methine and methylene $^1H-^{13}C$ bond vectors of *E. coli* thioredoxin[4] were modeled according to eq 7. Separate Monte Carlo analyses were carried out assuming from one to four Lorentzian terms for intermediate frequency internal motion, with their characteristic frequencies randomly selected between the bounds of $a\omega_{H+C}$ and $b\omega_C$. The calculations were repeated for differing values of a and b. The parameters a and b were varied to obtain the maximal range for which the root-mean-square deviation (rmsd) of the predicted S^2 and S_f^2 values are generally smaller than the anticipated uncertainty in the experimental relaxation data.

For each case of one to four Lorentzian terms, 3×10^8 sets of independent values of S^2, S_f^2 and the Lorentzian amplitude and time constants were tested against each set of experimental (T_1,T_2,NOE) values, with uncertainty bounds of 1% for T_1 and T_2 and 0.01 for NOE. Use of 0.5% and 0.005, respectively, for the T_1, T_2, and NOE uncertainty bounds did not significantly affect the results of the subsequent analysis. In the first round of Monte Carlo analysis, the random selection of test amplitudes was constrained only by the normalization of their sum. For the sets of experimental (T_1,T_2,NOE) values which were not satisfied by at least 10^4 sets of dynamical parameters, a second round of Monte Carlo analysis was performed. In the second round of Monte Carlo analysis, the range of S^2 and S_f^2 tested for each experimental (T_1,T_2,NOE) triplet was set to twice the range obtained in the first round (3 times that range if less than 100 sets of dynamical parameters passed the first round). In no case during the second round of Monte Carlo analyses did the extremum of the predicted S^2 and S_f^2 values come within 30% of these range limits. For each experimental (T_1,T_2,NOE) triplet, the mean and standard deviation of the derived S^2 and S_f^2 values were determined for all sets of dynamical parameters consistent with the (T_1,T_2,NOE) triplets for one to four independent Lorentzian terms.

Optimal frequency boundaries of $4\omega_{H+C}$ and $0.5\omega_C$ were obtained. For these experimental data obtained at 14.1 T, the corresponding time constants are 53 ps and 2.1 ns, respectively. Appreciable extensions of the frequency range in either direction results in a substantial decrease in the constancy of the S^2 and S_f^2 values predicted by the multiexponential expansion representation. The standard deviations for S^2 and S_f^2 are plotted in Figure 2A and B, respectively. The symbols for the calculated standard deviations are placed at the positions corresponding

(48) Woessner, D. E. *J. Chem. Phys.* **1962**, *36*, 1.
(49) Wittebort, R. J.; Szabo, A. *J. Chem. Phys.* **1978**, *69*, 1722.
(50) London, R. E.; Avitabile, J. *J. Am. Chem. Soc.* **1978**, *100*, 7159.
(51) Kinoshita, K.; Kawato, S.; Ikegami, A. *Biophys. J.* **1977**, *20*, 289.
(52) Lipari, G.; Szabo, A. *Biophys. J.* **1980**, *30*, 489.
(53) Perico, A.; Pratolongo, R. *Macromolecules* **1997**, *30*, 5958.
(54) Edholm, O.; Blomberg, C. *Chem. Phys.* **1979**, *42*, 449.
(55) Pratolongo, R.; Perico, A.; Freed, K. F.; Szabo, A. *J. Chem. Phys.* **1995**, *102*, 4683.
(56) Ziel, A. v. d. *Physica* **1950**, *16*, 359.
(57) Stein, D. *Proc. Natl. Acad. Sci. U.S.A.* **1985**, *82*, 3670.
(58) Ansari, A.; Berendzen, J.; Bowne, S. F.; Frauenfelder, H.; Iben, I. E. T.; Suke, T. B.; Shyansunder, E.; Young, R. D. *Proc. Natl. Acad. Sci. U.S.A.* **1985**, *82*, 5000.
(59) Bryngelson, J. D.; Wolynes, P. G. *Proc. Natl. Acad. Sci. U.S.A.* **1987**, *84*, 7524.
(60) Power, L. S.; Blumberg, W. E. *Biophys. J.* **1988**, *54*, 181.
(61) Sasai, M.; Ohmine, I.; Ramaswamy, R. *J. Chem. Phys.* **1992**, *96*, 3045.
(62) Takano, M.; Takahashi, T.; Nagayama, K. *Phys. Rev. Lett.* **1998**, *80*, 5691.

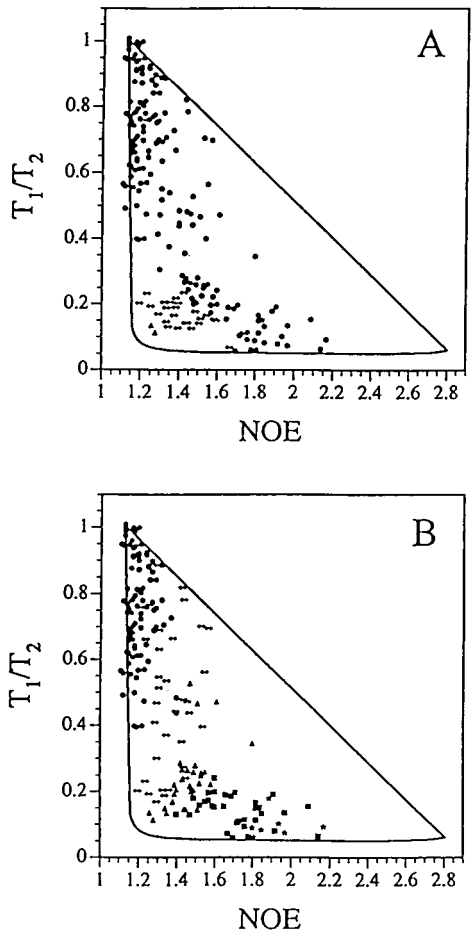

Figure 2. Calculation of the standard deviations for the S^2 (panel A) and S_f^2 (panel B) values estimated by applying the multi-Lorentzian spectral density formula of eq 7 to relaxation data from 201 methine and methylene resonances of *E. coli* thioredoxin. The symbols are plotted at the experimentally observed T_1/T_2 (normalized to the rigid tumbling limit value) vs NOE values with standard deviation values of less than 0.01 (●), 0.01−0.02 (↔), 0.02−0.03 (▲), 0.03−0.04 (■), and over 0.04 (★). The mean and standard deviations for the S^2 and S_f^2 values were determined assuming from one to four Lorentzians for the internal motion representation. These were combined with equal weighting to determine the aggregate standard deviations. In general, the difference between the mean predicted S^2 and S_f^2 values for $N = 1$ vs $N = 2$ is roughly twice that between $N = 2$ and $N = 3$, while the values for $N = 3$ and $N = 4$ are nearly converged. The series was truncated at $N = 4$ as the use of higher numbers of Lorentzians did not further change the estimated means and standard deviations from the $N = 4$ case. The differences between the mean predicted S^2 and S_f^2 values for differing numbers of Lorentzians and the dispersion of the predicted S^2 and S_f^2 values for a given number of Lorentzians ($N > 1$) generally contribute nearly equally to the aggregate standard deviation estimates illustrated in Figure 2. The boundary curve represents the full range of T_1/T_2 vs NOE values consistent with an arbitrary multiexponential autocorrelation function in which decay rates faster than $1/4\omega_{H+C}$ are combined into the fast limit order parameter. The calculations for this curve are based on a $^1H^2H^{13}C$ spin system.[4] The corresponding curve for a $^1H^{13}C$ spin system has the apex of the triangle shifted 0.03 higher in NOE, while the right-hand corner is displaced 0.1 higher in NOE due to the absence of the competing $^2H-^{13}C$ dipole interaction.

to the experimental values of T_1/T_2 (normalized to the rigid tumbling limit value) vs NOE. For the various individual experimental (T_1,T_2,NOE) triplets, the maximum range vs the standard deviation of the predicted S^2 and S_f^2 values were compared and found to be consistent with an approximately Gaussian distribution.

The triangular pattern in Figure 2 defines the boundaries of all T_1/T_2 vs NOE values consistent with an arbitrary multiexponential expansion representation of the internal autocorrelation function, assuming $1/4\omega_{H+C} < \tau_i < 1/0.5\omega_C$. Extending the contour to $\tau_i = 0$ increases the NOE value at the right-hand corner by 0.05. Only for rather mobile positions (i.e., normalized $T_1/T_2 < 0.25$) does the range of exponential amplitudes and time constants compatible with the experimental data appreciably deteriorate the precision of the S^2 (>0.01) and S_f^2 (>0.025) determinations. Uncertainty in the S^2 estimates (Figure 2A) is exacerbated at low NOE values, as expected since this is indicative of a predominance of internal motion that is slow compared to ω_{H+C}. The uncertainty of the S^2 estimates for this range of T_1/T_2 and NOE values rises nearly 2-fold if the low-frequency limit for the exponential sum of eq 7 is reduced to $0.33\omega_C$. Conversely, the uncertainty in the S_f^2 estimates increases for larger experimental NOE values, as expected for a predominance of internal motion near ω_{H+C}.

For the relaxation data of Figure 2, both the means and standard deviations for the S^2 and S_f^2 values derived from an analysis using only the two-Lorentzian internal motion representation of eq 7 closely approximate those obtained assuming equal weighting of the $N = 1$, 2, 3, and 4 Lorentzian representations. Indeed, for these relaxation data, the previously proposed two-Lorentzian internal motion representation[4,9] assuming fixed time constants of $1/\omega_{H+C}$ and $1/\omega_C$ predicts S^2 values which deviate from those of the full $N = 1$, 2, 3, 4 Lorentzian estimates by a maximum of 0.02 and an rmsd of 0.004. Similarly, this earlier simplified Larmor frequency-selective representation predicts S_f^2 values which deviate from those of the full $N = 1$, 2, 3, 4 Lorentzian estimates by a maximum of 0.04 and an rmsd of 0.008. On the other hand, the 1-to-1 mapping of the three-parameter dynamical formalisms onto the three experimental relaxation values precludes the use of these simplified formalisms in estimating the intrinsic imprecision of the order parameter estimates arising from an arbitrary multiexponential representation of the autocorrelation function. Although, based on the relaxation data of Figure 2, the two-Lorentzian internal motion representation of eq 7 appears to provide reliable estimates of the intrinsic imprecision of the order parameters, in general it is recommended to use the full $N = 1$, 2, 3, 4 Lorentzian analysis for deriving these estimates. By including up to the four-Lorentzian representation, more complex multiexponential autocorrelation function behavior potentially unrepresented in the data of Figure 2 should still be adequately modeled.

The wide range of mutual compensating shifts in the individual amplitudes for the $N = 2$, 3, and 4 representations of eq 7 provides some insight into how the robustness of the S^2 and S_f^2 estimates is achieved. The individual amplitudes for the two-Lorentzian internal motion representation is illustrated in Figure 3 for the case of Asp 13 $^1H^{\beta 2}-^{13}C^{\beta}$ vector. Here, 155 pairs of internal motion Lorentzians were randomly generated which fit the T_1, T_2, and NOE values for the Asp 13 $^1H^{\beta 2}-^{13}C^{\beta}$ vector to within 0.005. Following eq 7, the sum of the amplitudes of these two Lorentzians equals $S_f^2 - S^2$ (i.e., (+)). For each pair of Lorentzians illustrated, the lines connect the amplitudes for the low (×) and high (●)-frequency components. The pairs have been sorted in order of decreasing S^2 values. It is readily apparent that the amplitudes of the low- and high-frequency Lorentzian components fluctuate far more than does their sum. The rise in the ($S_f^2 - S^2$) values at the right side of the figure reflect the sampling of low-frequency components near the $0.5\omega_C$ partition boundary. The resultant ambiguity in

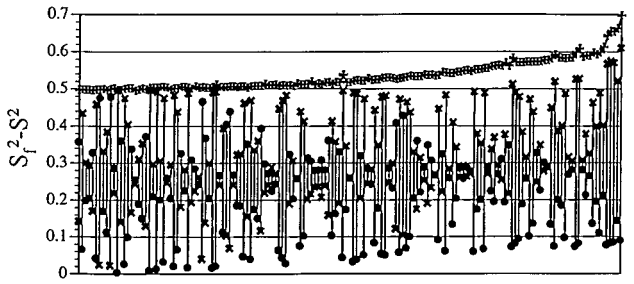

Figure 3. Individual Lorentzian amplitudes for the two-Lorentzian internal motion representation (eq 7) for the relaxation data of the Asp 13 $^1H^{\beta 2}-^{13}C^{\beta}$ dipole. The low (×)- and high (●)-frequency Lorentzian amplitude components are illustrated along with their sum, which defined as $S_f^2-S^2$ (+). The 155 randomly selected individual amplitude pairs are ordered according to the descending value of the predicted S^2. The increase in the $S_f^2 - S^2$ values in the right-hand portion of this figure reflects the presence of high-amplitude values for the low-frequency components which are near the $0.5\omega_C$ frequency boundary.

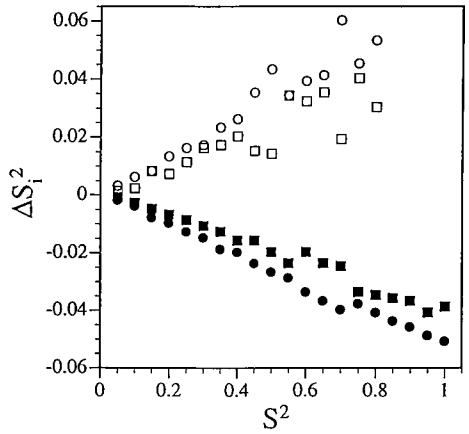

Figure 4. Average errors in S_f^2 (circles) and $S_f^2 - S^2$ (squares) estimation for global tumbling times 10% shorter (open symbols) and 10% longer (closed symbols) than optimal. Order parameter calculations were conducted as in Figure 2 for the same relaxation data set. The deviations from the S_f^2 and $S_f^2 - S^2$ values obtained for the optimal t_M are plotted against the optimal S^2 values. The individual values were averaged in bin intervals of 0.05. In the case of the 10% foreshortened τ_M when the S^2 value is above 0.8, the relaxation data lie outside the range consistent with the multiexponential internal correlation function representation.

partitioning between internal and global dynamics is largely responsible for the comparatively high estimated uncertainty in the S^2 value for this C^{β}. In addition to the mutual compensating shifts of the individual Lorentzian amplitudes required to maintain an approximately constant sum, corresponding shifts in the individual time constants occur simultaneously in order to maintain the required fit to the experimental data.

In marked contrast to the robustness of the S^2 and S_f^2 estimates over a wide range of dynamical parameters, the apparent time constants are more poorly determined. One measure of this dispersion is the standard deviation of the time constant for the largest amplitude internal motion Lorentzian term in eq 7. For the 201 (T_1,T_2,NOE) values in Figure 2, the median standard deviation of the dominant time constant is 60%. Despite the obvious appeal of using the relaxation data to extract conformational transition rates, the variability of both the individual Lorentzian amplitudes and time constants consistent with the predicted ($S_f^2 - S^2$) values argues strongly against such physical interpretations, except for cases in which independent evidence indicates a single dominant dynamic process.

In addition to the spectral density formula of eq 7 based on a multiexponential internal autocorrelation function, the only other necessary assumption of this analysis is that of the separability of the internal and global tumbling dynamics. Clearly, errors in the analysis of global tumbling will result in distortion of the estimated internal dynamics parameters. Qualitatively, it can be anticipated that such distortions will be most severe for positions exhibiting limited internal mobility, since in these cases the global tumbling contributes most strongly to the relaxation behavior.

To examine these effects in more detail, the calculations of Figure 2 were repeated using global tumbling times 10% higher and 10% lower than the optimal value. In Figure 4 is illustrated the average deviation of the apparent ($S_f^2 - S^2$) and S_f^2 values from the order parameter values obtained in the analysis of Figure 2 as a function of the S^2 value. The 10% error in global tumbling time results in approximately a 10% error in the estimated S^2 value, with an underestimate occurring for the overly long tumbling time and an overestimate occurring for the foreshortened tumbling time. For small values of S^2, these errors constitute fairly modest differences in the estimated generalized order parameter. On average, the deviations in the estimated S^2 values are compensated for nearly equally by corresponding deviations in the estimated ($S_f^2 - S^2$) and S_f^2 values. When analyzing positions with S^2 values above 0.8 using the 10% foreshortened global tumbling times, the relaxation values no longer lie within the triangle predicted by the multiexponential internal autocorrelation function. The potential misinterpretation of these data in terms of chemical exchange broadening can be directly tested by field strength dependence or spin-lock studies.

The intrinsic imprecision in the determination of S^2 and S_f^2 resulting from applying the multiexponential expansion to precise data values was analyzed above in Figure 2. A proper estimate of experimental order parameter uncertainty is obtained by applying the multiexponential expansion analysis to the relaxation data with the experimentally determined uncertainties assigned. The practical utility of this dynamical representation is demonstrated by the fact that, for most resonances, the derived uncertainty of their order parameters primarily reflects the magnitude of the experimental uncertainties in the relaxation data rather than the magnitude of the intrinsic imprecision of the dynamical representation.

The potential limitations of the frequency partitioning used in eq 7 can be further probed by consideration of frequency components which occur near the range boundaries. Regarding the high-frequency boundary, dynamical processes having time constants more than 10−20 times shorter than $1/\omega_{H+C}$ (i.e., ∼10 ps) do not have a discernible differential effect on the spectral density components sampled by the NMR experiment. As time constants between ∼10 and ∼50 ps represent a transition range for which experimental characterization as either fast limit or Larmor frequency sensitive motion is ambiguous, it is instructive to consider cases in which such a motion is analyzed in terms of the frequency-bounded multi-Lorentzian formalism of eq 7. When relaxation data are synthesized from single-exponential autocorrelation functions with time constants in the range of 10−50 ps and then analyzed according to the multi-Lorentzian formalism with a $4\omega_{H+C}$ boundary, it is found that the amplitude of the single-exponential component is partitioned between S_f^2 and ($S_f^2 - S^2$) approximately proportionate to the position of that exponential time constant within the 10−50-ps interval.

Assessing the limitations of partitioning at the low-frequency boundary is more problematic since, as is apparent in eq 5, internal frequency components approximately equal to the molecular tumbling frequency cannot yield independent ampli-

tude predictions. Hence, the S^2 value derived from this formalism is necessarily an upper bound. In the case of the 7-ns molecular tumbling time of *E. coli* thioredoxin considered herein, the $0.5\omega_C$ frequency boundary implies an approximate 4-fold range in frequency for internal motions which are not well characterized. The predicted dominant time constant provides a means of detecting potential motion slower than the partition boundary. For all resonances having a predicted dominant time constant more than 2-fold faster than that of the low frequency boundary, extension of low-frequency boundary from $0.5\omega_C$ to $0.33\omega_C$ changed the estimated S^2 by less than 0.01. For resonances having predicted dominant time constants nearer to the low-frequency boundary and relatively large intermediate frequency motion $S_f^2 - S^2$, truncation effects should be suspected, and use of a lower frequency boundary should be considered.

In contrast to the $4\omega_{H+C}$ high-frequency partition which is expected to be of general use for protein analysis, the optimal choice of the low-frequency partition can be anticipated to be modestly affected by the molecular tumbling time. For substantially differing molecular tumbling times, a comparison between the intrinsic imprecision in the multiexponential expansion and the experimental uncertainity of the relaxation data should be conducted. Analogous considerations will apply to the application of this formalism to ^{15}N relaxation data.

IIIA. Fast Limit Order Parameter Distribution for *E. coli* Thioredoxin

The order parameter analysis presented above represents the internal autocorrelation function in terms of a fast limit decay and an arbitrary multiexponential expansion composed of decay rates ranging from $4.\omega_{H+C}$ to $0.5.\omega_C$. At 14.1 T, this 40-fold difference corresponds to a time constant range from 53 ps to 2.1 ns. Robust estimates are obtained for both the fast limit order parameter characterizing motions that are rapid compared to the highest Larmor frequency ω_{H+C}, and the generalized order parameter, characterizing the rotational disorder arising from the global molecular tumbling.

An obvious question which arises regards the degree to which the fast limit order parameter S_f^2 corresponds to dynamics within localized potential minima and the degree to which larger scale conformational transitions contribute predominantly to the difference order parameter $S_f^2 - S^2$. A qualitative indication of the plausibility of such a partitioning can be obtained by consideration of the overall distribution of S_f^2 values throughout the protein structure. *E. coli* thioredoxin exhibits typical main-chain dynamics in which the vast majority of ^{15}N and $^{13}C^\alpha$ resonances have $0.8 < S^2 < 0.9$,[4,35] indicative of limited dynamic angular disorder. Furthermore, in most cases the main-chain $S_f^2 - S^2$ values are small, indicating that fast limit dynamics dominate the angular disorder. As described in more detail in section IV, assuming an S_f^2 value of 0.8, the order parameter values at C^β and C^γ can be estimated for the case of unrestricted side-chain torsional fluctuations within a given rotamer state. The resultant S_f^2 values of ~0.68 for C^β and ~0.52 for C^γ (assuming 3-fold rotational barriers) should represent a lower bound for the fast limit order parameters of the side chains attached to a moderately immobilized C^α position if only fluctuations within a rotamer state contribute significantly to the observed S_f^2 values.

With the exception of the highly mobile N-terminal serine and the four trans prolines, all methine and methylene C^β positions of *E. coli* thioredoxin have S_f^2 values above 0.65 (Lys 57 C^β). Similarly, the 0.50 C^γ S_f^2 value of Lys 69 is the lowest non-proline C^γ S_f^2 value in the protein. Hence, all non-proline side chains exhibit fast limit order parameters, consistent with dynamics within a given rotamer state, and indeed the observed lower bounds correspond quite closely to the lower bound anticipated for that dynamical model. In contrast, all four trans prolines exhibit C^β S_f^2 values below 0.65 and C^γ S_f^2 values below 0.51.

The explanation of the anomolous behavior of the proline side chains is provided by the solid-state NMR observation that the proline ring pucker transition occurs with a time constant of 10−30 ps.[63] The pattern of order parameters of $C^\delta > C^\beta > C^\gamma$ predicted and observed in small proline-containing peptides[64] is also observed for all of the prolines in *E. coli* thioredoxin, including the anticipated higher order parameters for the single cis Pro 76.[4] As all four trans prolines have C^α S^2 values above 0.83, and their low side-chain S_f^2 values are clearly indicative of rapid motion of a magnitude larger than simple fluctuation within a rotamer state. The proline-ring puckering dynamics lie in the boundary range between the highest frequency quantitated by the multiexponential autocorrelation function expansion (i.e., $4\omega_{H+C} \approx 50$ ps) and the true fast limit range, in which the relaxation effects are insensitive to the Larmor frequencies (i.e., $<\sim 10$ ps). Assuming a two-state pucker transition to rationalize the proline relaxation data, the partitioning of the motion between the S_f^2 and ($S_f^2 - S^2$) values is consistent with a transition time constant in the range of 20−30 ps.

An analogous situation occurs for the methyl groups in which the 3-fold rotation around the symmetry axis gives rise to a predictable order parameter effect, 0.111 for an ideal tetrahedral geometry. The derived methyl S_f^2 values are consistently lower than that expected from fluctuation in a single rotamer state, indicative of the fact that the methyl rotamer transitions are contributing to the S_f^2 values, consistent with previous measurements indicating that methyl rotation occurs at a rate near the boundary of the multiexponential autocorrelation function frequency partitioning.[65] The multiexponential autocorrelation function frequency partitioning cleanly distinguishes the two best-characterized cases in which the S_f^2 values could be anticipated to exhibit intermixing of intrarotamer fluctuations and larger scale conformational transitions. These results are strongly suggestive of the utility of this formalism for analysis of more complex dynamical behavior.

IIIB. Quasiharmonic Analysis of Correlated Side-Chain Motion

Correlated motion arises from the restriction of mobility due to either intramolecular or solvent−solute interactions. Rotational correlations generally serve to minimize the displacements of all atoms.[66] This effect is opposed by the thermodynamic drive to increase configurational entropy by maximizing the magnitude of the uncorrelated motion. Under the quasiharmonic approximation, the magnitude of both correlated and uncorrelated fluctuations is characterized by the covariance matrix σ of the internal coordinates q with elements $\sigma_{ij} = \langle (q_i - \langle q_i \rangle)(q_j - \langle q_j \rangle) \rangle$.[67] Assuming classical dynamics, the configurational

(63) Sarkar, S. K.; Young, P. E.; Torchia, D. A. *J. Am. Chem. Soc.* **1986**, *108*, 6459.
(64) London, R. E. *J. Am. Chem. Soc.* **1978**, *100*, 2678.
(65) Daragan, V. A.; Mayo, K. H. *J. Magn. Reson. Ser. B* **1996**, *110*, 164.
(66) Helfand, E. *Science* **1984**, *226*, 647.
(67) Karplus, M.; Kushick, J. N. *Macromolecules* **1981**, *14*, 325.

entropy difference ΔS_q^c depends only on the determinant of this matrix for the individual conformational states.

$$\Delta S_q^c = {}^1/_2 k_B \ln[\det \sigma_B / \det \sigma_A] \quad (8)$$

Quantum mechanical corrections to the quasiharmonic configurational entropy introduce only an additive constant to each determinant term in this expression.[68] Quantum mechanical corrections to order parameter calculations introduce a uniform decrease due to the bond length and bond angle fluctuations at the H−X bond.[69] For the dihedral angle space Monte Carlo simulations considered below, additional quantum mechanical corrections to the order parameters are negligible.[70]

As the covariance matrix is symmetric semidefinite, it can be diagonalized by an orthogonal transformation. The resultant diagonal elements are the variances of the uncorrelated fluctuations for each of the internal coordinates, consistent with the general fact that only the uncorrelated fluctuations will contribute to the configurational entropy. As a result of the Gaussian distribution which arises from a parabolic potential, the configurational entropy predicted from the quasiharmonic approximation represents the upper bound of the configurational entropy consistent with a given variance of the conformational fluctuations.[71]

In contrast to the complex network of correlated motions characterizing protein main-chain fluctuations, it is plausible to model the torsional dynamics of the buried side chains in a simpler fashion. The surrounding protein matrix imposes an effective diffusive barrier. The side chain will tend to maximize its uncorrelated fluctuations within this potential well. However, the torsional fluctuations of the main-chain atoms restrict the range of side-chain torsional fluctuations compatible with the steric constraints of the protein matrix, thus imposing correlated motion.

A further simplication of the present analysis is to freeze the "hard" variables of bond lengths and bond angles and consider only the effects of "soft" torsional fluctuations.[72] Bond angle fluctuations can make a significant contribution to the configurational entropy.[67] However, since this formalism is designed to estimate differences in configurational entropy, only the variation in bond angle fluctuations which are induced by restricted torsional fluctuations will affect the calculations. As the free energy of the torsional restrictions considered herein is reasonably modest ($\sim k_B T$), the entropy contributions of differential bond angle fluctuations are anticipated to be comparatively small.

Illustrating for the case of two side-chain dihedral angles, the correlated motion is represented by the correlation coefficients for the torsional fluctuations of the main-chain, χ_1, and χ_2 dihedral angles. As vindicated by the calculations given below, the dominant correlations can be expected for the main-chain dihedral angle for which the corresponding bond vector is approximately parallel to the $C^\beta-C^\gamma$ bond, thus allowing for "crankshaft" type coupling of the main-chain and χ_2 fluctuations. Such crankshaft motions are well-known to play a dominant role in the conformational dynamics of linear polyethylene-like polymers.[66]

With the additional assumption that the correlation between χ_1 and χ_2 fluctuations occur only via their mutual correlations with the main chain, for a side chain having a χ_1 value near 180°, the corresponding covariance matrix is

$$\begin{bmatrix} \sigma_\phi^2 & c_{\phi\chi_1}\sigma_\phi\sigma_{\chi_1} & c_{\phi\chi_2}\sigma_\phi\sigma_{\chi_2} \\ c_{\phi\chi_1}\sigma_\phi\sigma_{\chi_1} & \sigma_{\chi_1}^2 & c_{\phi\chi_1}c_{\phi\chi_2}\sigma_{\chi_1}\sigma_{\chi_2} \\ c_{\phi\chi_2}\sigma_\phi\sigma_{\chi_2} & c_{\phi\chi_1}c_{\phi\chi_2}\sigma_{\chi_1}\sigma_{\chi_2} & \sigma_{\chi_2}^2 \end{bmatrix} \quad (9)$$

The resultant eigenvalues are σ_ϕ^2, $(1 - c_{\phi\chi_1}^2)\sigma_{\chi_1}^2$, and $(1 - c_{\phi\chi_2}^2)\sigma_{\chi_2}^2$ where c_{ij} is the correlation coefficient $\langle \Delta i \Delta j \rangle / \langle \Delta i^2 \rangle^{0.5} \langle \Delta j^2 \rangle^{0.5}$, with Δi representing the deviation of the torsional angle from its mean position and σ_i is the rmsd of the torsional fluctuation. Note that, by assumption, $c_{\chi_1\chi_2} = c_{\phi\chi_1}c_{\phi\chi_2}$. For χ_1 values near −60°, the main-chain ψ dihedral angle is substituted for ϕ. For leucine and phenylalanine residues, as considered below, over 90% of the observed χ_1 values are near either −60° or 180°.[73]

The covariance matrix of eq 9 contains three torsional fluctuations and two correlation coefficients which need to be estimated from the experimental relaxation data. Generally this will represent an underdetermined system. Given the main-chain torsional fluctuation, a four-dimensional grid of Monte Carlo simulations can be carried out to determine the range of side-chain torsional fluctuations and correlation coefficients consistent with the experimental data. Gaussian sampling of the main-chain, χ_1, and χ_2 torsional angle distributions are constructed so that the degree of correlation of the side-chain torsional fluctuations to those of the main chain is systematically adjusted.

Although a physically plausible model for the side-chain fluctuations can be so simply described, specification of the relevant main-chain torsional fluctuation is more problematic. Comparison to the experimental $^{13}C^\alpha$ relaxation data requires a modeling of the local main-chain motion. The simplest model ascribes all of the $^{13}C^\alpha$ relaxation to the fluctuation of a single main-chain torsional angle. This model has the conceptual appeal that, for side-chain dynamics dominated by a crankshaft type of fluctuation, the maximum range of side-chain fluctuations is predicted. More realistic is to assume correlated intraresidue (ϕ,ψ) motion, for which molecular dynamics simulations have indicated a correlation coefficient of approximately −0.5 for α-helical residues.[74,75] Although the introduction of correlated intraresidue (ϕ,ψ) motion serves to reduce the range of side-chain fluctuations consistent with experimental relaxation data considered below, it does not substantially affect the predicted degree of correlation and hence the conformational entropy for the residual permitted range of side-chain fluctuations.

IIIC. Correlated Motion of Buried Side Chains

Phe 12 of *E. coli* thioredoxin has $H^\alpha-C^\alpha$, $H^{\beta2}-C^\beta$, $H^{\beta3}-C^\beta$, and $H^\delta-C^\delta$ S^2 order parameters of 0.82, 0.78, 0.79, and 0.93, respectively.[4] As the S_f^2 values are not statistically different, the relevant internal motion occurs in the fast limit regime. Using the crystallographically observed χ_1 and χ_2 dihedral angles (−158,92),[36] Monte Carlo simulations were carried out as a function of dihedral angle variances and correlation coefficients to determine combinations consistent with the observed relaxation order parameters. The main-chain ϕ rotation axis is approximately parallel to the $C^\beta-C^\gamma$ bond vector, so that crankshaft coupling of ϕ and χ_2 torsional fluctuations is anticipated. In the initial round of simulations, the C^α order parameter was interpreted in terms of only ϕ torsional fluctua-

(68) Schlitter, J. *Chem. Phys. Lett.* **1993**, *215*, 617.
(69) Bruschweiler, R. *J. Am. Chem. Soc.* **1992**, *114*, 5341.
(70) Sunada, S.; Go, N.; Koehl, P. *J. Chem. Phys.* **1996**, *105*, 6560.
(71) Rojas, O. L.; Levy, R. M.; Szabo, A. *J. Chem. Phys.* **1986**, *85*, 1037.
(72) Go, N.; Scheraga, H. A. *J. Chem. Phys.* **1969**, *51*, 4751.
(73) Ponder, J. W.; Richards, F. M. *J. Mol. Biol.* **1987**, *193*, 775.
(74) Daragan, V. A.; Mayo, K. H. *J. Phys. Chem.* **1996**, *100*, 8378.
(75) Garnier, N.; Genest, D.; Genest, M. *Biophys. Chem.* **1996**, *58*, 225.

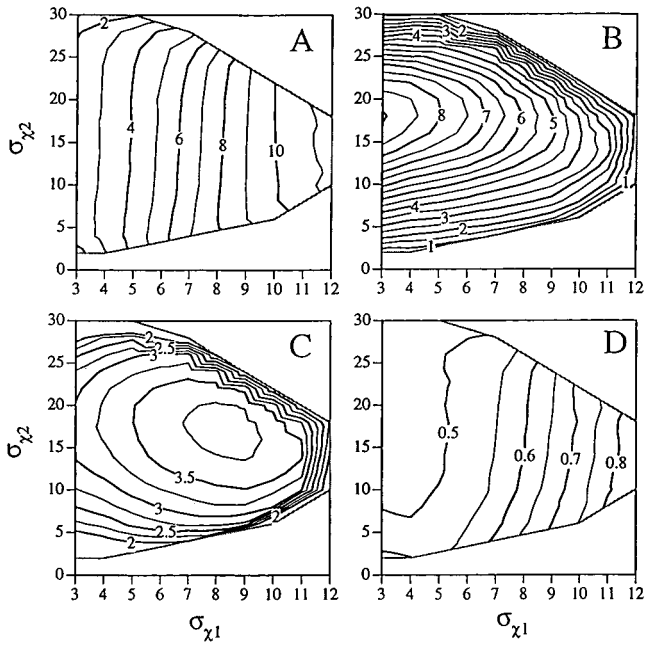

Figure 5. Side-chain torsional dynamics of *E. coli* thioredoxin Phe 12 assuming correlated fluctuations for (ϕ,χ_1) and (ϕ,χ_2) in which the Gaussian main-chain ϕ fluctuations have a σ_ϕ of 16° (predicts C^α S^2 of 0.82) and ψ is fixed. Panels A and B illustrate the magnitude (in degrees) of uncorrelated χ_1 and χ_2 fluctuations, respectively, as a function of the total torsional fluctuations σ_{χ_1} and σ_{χ_2}. The corresponding quasiharmonic relative side-chain torsional configurational entropy and side-chain heavy-atom rmsd are given in panels C and D. For each set of (σ_{χ_1},σ_{χ_2},$c_{\phi\chi_1}$,$c_{\phi\chi_2}$) values, 10^4 different side chain conformations were generated, and the resultant order parameters calculated. The set of all (σ_{χ_1},σ_{χ_2},$c_{\phi\chi_1}$,$c_{\phi\chi_2}$) values which predict the experimental order parameters with a χ^2 probability of >0.05 were determined. The values given in the figure for each (σ_{χ_1},σ_{χ_2}) pair were obtained by summing over the ($c_{\phi\chi_1}$,$c_{\phi\chi_2}$) values weighted according to their χ^2 probability.

tions. It should be noted that, for S^2 values greater than 0.6, the order parameter relationship of eq 1 can be further simplified to state that S^2 depends only on the variance of the H−X bond orientation, regardless of whether the bond motion occurs via discrete jumps or by one- or two-dimensional diffusion.[76] As a result, the direction of motion providing the largest variance will generally dominate the determination of the corresponding order parameter.

A Gaussian fluctuation σ_ϕ of 16° predicts the observed 0.82 C^α order parameter.[12] χ_1 and χ_2 values were selected so that their population mutually satisfied the constraints of a given σ_i and a given correlation coefficient with the ϕ angle values. A grid search was conducted over the total torsional fluctuations σ_{χ_1} and σ_{χ_2} and the corresponding correlation coefficients $c_{\phi\chi_1}$ and $c_{\phi\chi_2}$ with the main-chain ψ dihedral angle fixed. For each set of (σ_{χ_1}, σ_{χ_2}, $c_{\sigma\chi_1}$, $c_{\sigma\chi_2}$) values, 10^4 different side-chain conformations were generated. Calculation of the corresponding order parameters was facilitated by use of the explicit representation of the spherical harmonics in terms of Cartesian coordinates.[77] Using the estimated experimental uncertainties of the Phe 12 relaxation data applied to the multiexponential order parameter analysis, the set of all (σ_{χ_1}, σ_{χ_2}, $c_{\sigma\chi_1}$, $c_{\sigma\chi_2}$) values predicting the experimental order parameters with a χ^2 probability in excess of 0.05 were determined. For each (σ_{χ_1}, σ_{χ_2}) value in Figure 5, the individual data points are derived by averaging over the ($c_{\sigma\chi_1}$, $c_{\sigma\chi_2}$) values with weighting according to the predicted χ-square probability.

The average magnitude of uncorrelated χ_1 and χ_2 torsional fluctuations (i.e., sqrt[$(1 - c_{\phi\chi_1}{}^2)\sigma_{\chi_1}{}^2$] and sqrt[$(1 - c_{\phi\chi_2}{}^2)\sigma_{\chi 2}{}^2$], respectively) as a function of total χ_1 and χ_2 torsional fluctuations σ_{χ_1} and σ_{χ_2} are plotted in panels A and B of Figure 5, respectively. As anticipated for crankshaft-like dynamics, quite large fluctuations of χ_2 are consistent with the rigidly constrained aromatic ring (panel B). For any given value of σ_{χ_1}, as the χ_2 fluctuations increase, the magnitude of uncorrelated fluctuations reaches a maximum and then declines, indicative of increasingly strong anticorrelation between ϕ and χ_2 fluctuations. In contrast, σ_{χ_1} is restricted to values well below the approximate 18° limit imposed by the local rotamer potential well of such an sp^3-sp^3 system (panel A). Furthermore, as illustrated in this panel, the χ_1 fluctuations are comparatively weakly correlated with those of ϕ, as indicated by the predicted magnitude of the uncorrelated χ_1 fluctuations being nearly as large as the magnitude of the total χ_1 fluctuations σ_{χ_1}.

In panel C of Figure 5, the determinant of eq 9 is used to estimate the relative side-chain torsional configurational entropy as a function of σ_{χ_1} and σ_{χ_2}. In panel D is given the predicted side-chain heavy atom rmsd for these fluctuations. For (σ_{χ_1}, σ_{χ_2}) values around (7°,18°), a near-maximal entropy is obtained with a side-chain heavy-atom rmsd of 0.55 Å, approximating the mean-square displacement commonly deduced from X-ray diffraction analysis and molecular simulations. For this (σ_{χ_1},σ_{χ_2}) pair, $c_{\phi\chi_1}$ is estimated to be 0.28, consistent with the average main-chain-χ_1 correlation coefficient from molecular dynamics simulations.[74] For the optimal (σ_{χ_1},σ_{χ_2}) value at (7°,18°), $c_{\chi_1\chi_2}$ is estimated to be approximately −0.25, consistent with molecular dynamics calculations for buried aromatic rings,[78] despite the fact that, in the present calculations, these correlations are assumed to arise only via their mutual coupling to ϕ fluctuations.

The corresponding analysis of Phe 12 dynamics assuming no torsional correlation yields no (σ_{χ_1},σ_{χ_2}) values predicting the experimental order parameters with χ^2 probabilities above 0.003. An analogous calculation assuming ψ−side-chain torsional correlation with the ϕ torsional angle fixed also yields no combinations fitting experimental side-chain order parameters with χ^2 probabilities above 0.003. As expected, the predominant limitation in both of these calculations is the inability to accommodate the high aromatic ring order parameter, except for implausibly small dihedral angle fluctuations.

Not only does the assumption of predominant correlation between ϕ and the side-chain dihedral angles appear well-vindicated, but also these results suggest that the fluctuations of the main-chain ψ torsional angle may be attenuated by its gauche orientation relative to the aromatic ring. This effect can be more realistically modeled allowing for correlated (ϕ,ψ) fluctuations. Molecular dynamics simulations of α-helical residues have indicated that the intraresidue (ϕ,ψ) fluctuations have a correlation coefficient of approximately −0.5.[74,75] Phe 12 lies within the α_1 helix of the protein. Assuming Gaussian torsional fluctuations with a $c_{\phi\psi}$ of −0.5 and both σ_ϕ and σ_ψ equal to 13° predicts the observed 0.82 C^α S^2 value. In Figure 6 are plotted the corresponding uncorrelated χ_1 (panel A) and χ_2 (panel B) fluctuations, along with the relative side-chain torsional entropy (panel C) and side-chain heavy-atom rmsd (panel D) for conditions analogous to those of Figure 5. As compared to the data of Figure 5, the heavy-atom rmsd is increased approximately 0.25 Å (panel D), and the range of χ_2

(76) LeMaster, D. M. *J. Biomol. NMR* **1997**, *9*, 79.
(77) Bremi, T.; Bruschweiler, R.; Ernst, R. R. *J. Am. Chem. Soc.* **1997**, *119*, 4272.
(78) McCammon, J. A.; Gelin, B. R.; Karplus, M. *Nature* **1977**, *267*, 585.

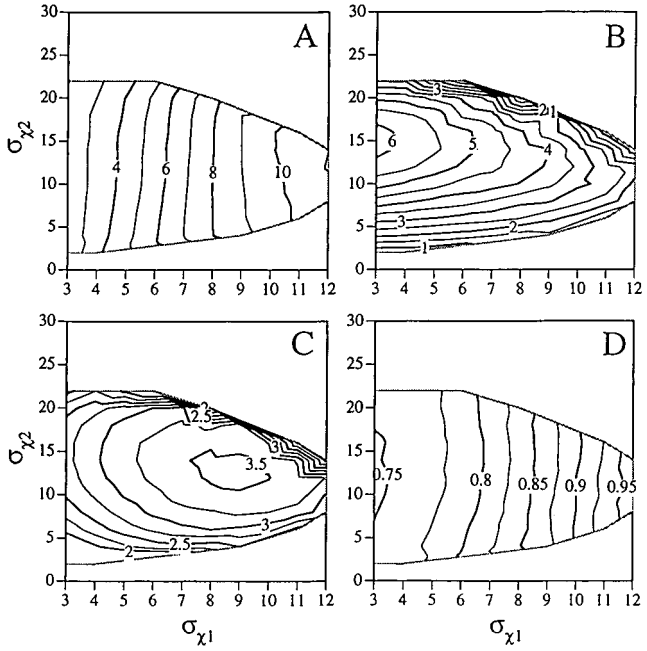

Figure 6. Side-chain torsional dynamics of *E. coli* thioredoxin Phe 12 assuming correlated fluctuations for (ϕ,χ_1) and (ϕ,χ_2) in which the ϕ and ψ fluctuations have equal σ values of 13°, with $c_{\phi\psi}$ of −0.5 (predicts C^α S^2 of 0.82). Panels A and B illustrate the magnitude of uncorrelated χ_1 and χ_2 fluctuations, respectively, as a function of the total torsional fluctuations σ_{χ_1} and σ_{χ_2}. Panels C and D illustrate the quasiharmonic relative side-chain torsional entropy and side-chain heavy-atom rmsd as calculated for Figure 5.

fluctuations consistent with the experimental order parameters is significantly reduced.

Minimization of the side-chain heavy-atom rmsd due to steric conflict with the protein interior provides the energetic drive for the correlated motion of the phenylalanine residue. The increase in the predicted side-chain heavy-atom rmsd resulting from analyzing the effects of increased ψ fluctuations further suggests that, reciprocally, the immobilization of the aromatic ring will cause a reduction in the main-chain ψ fluctuations relative to those of ϕ. These effects are further accentuated if the ϕ and ψ fluctuations are assumed to be uncorrelated.

On the other hand, within the permitted regions common to both Figures 5 and 6, the relative side chain torsional entropy values are fairly similar with and without the inclusion of ψ fluctuations, indicating that, for a given (σ_{χ_1}, σ_{χ_2}) pair, similar correlation coefficient values yield the best fit to the experimental order parameters. As the true values of σ_ϕ, σ_ψ, and $c_{\phi\psi}$ are anticipated to lie between those used for Figures 5 and 6, the data of these figures should provide a reliable estimate of the corresponding relative side-chain torsional entropy.

These model calculations may be contrasted to the recent NMR relaxation analysis of the dynamics of the solvent-exposed phenylalanine residues of the cyclic peptide antamanide.[77] In that study, the authors analyze the side-chain dynamics assuming a rigid peptide backbone. As explicitly verified by Monte Carlo simulations, under this assumption the order parameter of the aromatic C^δ can never be higher than that of C^β. The assumption of independent main-chain and side-chain dynamics is clearly inappropriate for the case of the structurally buried side chain. As discussed in more detail in section IV, the assumption of independent main-chain and side-chain dynamics appears to also be inappropriate, even in the case of highly solvated mobile side chains.

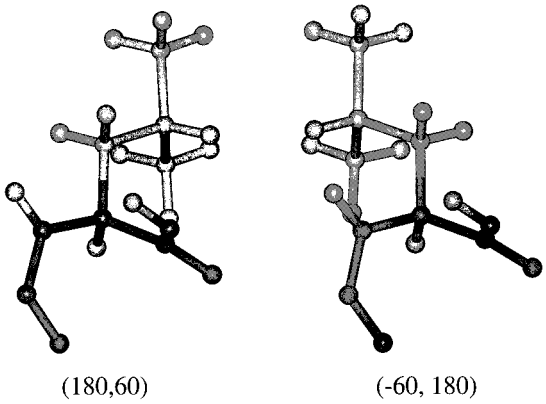

Figure 7. Illustration of the two most common leucine rotamers which are related to each other by a pseudomirror through the plane defined by $H^\alpha-C^\alpha-C^\beta$.

The side-chain dynamics of buried leucine residues provide a more demanding test for whether observed relaxation order parameters are consistent with fluctuations within a single rotameric state. Earlier relaxation studies[1,24] have interpreted the low and variable order parameters of the methyl rotation axes as indicative of large-scale internal dynamics, inconsistent with range of motion commonly inferred from analysis of X-ray Debye−Waller factors. A physically plausible mechanism of generating low order parameters for the leucine methyl rotation axes is illustrated in Figure 7. The two rotamers (−60,180) and (180,60) constitute 88% of all leucine rotamers observed in high-resolution X-ray structures.[73] These two rotamer states are related to each other by a pseudomirror through the plane defined by $H^\alpha-C^\alpha-C^\beta$. Dynamical interchange between these two rotamer states could potentially offer an efficient relaxation mechanism with a relatively modest rearrangement of the protein interior. Arguments based on molecular dynamics simulations have recently been used to rationalize the low leucine methyl axis order parameters of barstar in terms of such a rotamer transition.[79] The analysis of correlated torsional fluctuations described herein provides a means of determining whether fluctuations within a rotamer well are sufficient to rationalize the observed relaxation data, or whether a more extensive reorientation, such as that illustrated in Figure 7, must be invoked. This relaxation analysis provides a complement to spin-coupling studies[80−83] for characterizing heterogeneity in the torsional angle averaging.

The α-helical residue Leu 99 of *E. coli* thioredoxin offers a useful illustration of the present procedure, as the 0.37 order parameter of the *pro-R* methyl rotation axis is nearly the lowest for the 13 leucines of this protein, while the 0.63 order parameter of the *pro-S* methyl rotation axis represents the largest disparity between such intraresidue geminal order parameters. Given the mean (χ_1,χ_2) values of (−178,53) of this α-helical residue,[36] it is anticipated that ϕ−side-chain correlations will again dominate the torsional dynamics due to the crankshaft-like orientation of the ϕ and χ_2 rotation vectors.

Monte Carlo simulations were carried out assuming not only the expected correlated ϕ−side-chain fluctuation case, but also

(79) Wong, K. B.; Daggett, V. *Biochemistry* **1998**, *37*, 11182.
(80) Vuister, G. W.; Yamazaki, T.; Torchia, D. A.; Bax, A. *J. Biomol. NMR* **1993**, *3*, 297.
(81) Kariminejad, Y.; Schmidt, J. M.; Ruterjans, H.; Schwalbe, H.; Griesinger, C. *Biochemistry* **1994**, *33*, 5481.
(82) Kay, L. E.; Muhandiram, D. R.; Farrow, N. A.; Aubin, Y.; Forman-Kay, J. D. *Biochemistry* **1996**, *35*, 361.
(83) Konrat, R.; Muhandiram, D. R.; Farrow, N. A.; Kay, L. E. *J. Biomol. NMR* **1997**, *9*, 409.

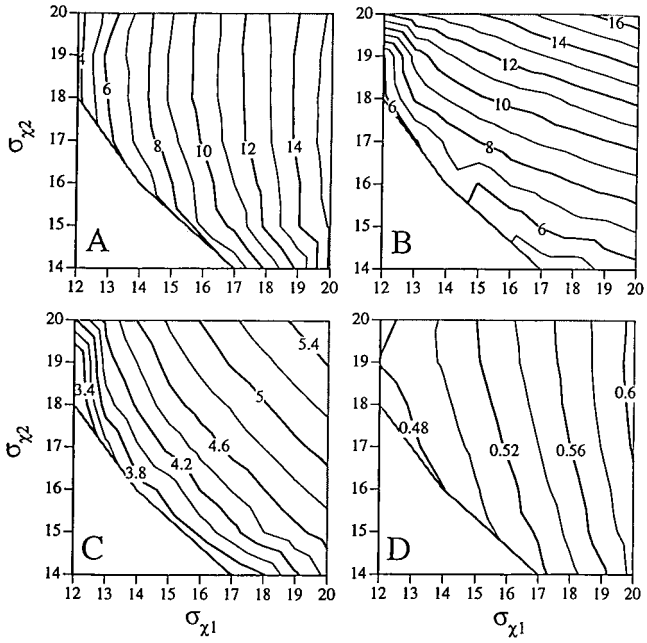

Figure 8. Side-chain torsional dynamics of *E. coli* thioredoxin Leu 99 assuming correlated fluctuations for (ϕ,χ_1) and (ϕ,χ_2) in which the ϕ fluctuations have a σ_ϕ of 10° (predicts C^α S^2 of 0.93) and ψ is fixed. Panels A and B illustrate the magnitude of the uncorrelated χ_1 and χ_2 fluctuations, respectively, as a function of the total side-chain torsion fluctuations. Panels C and D illustrate the quasiharmonic relative side-chain torsional entropy and side-chain heavy-atom rmsd as calculated for Figure 5.

correlated ψ−side-chain and correlated (ϕ,ψ)−side-chain torsional fluctuations. The most favorable combination of correlated ψ−side-chain fluctuations fails to predict the observed order parameters with a χ^2 probability well in excess of 0.99, consistent with the expected incompatibility of the gauche orientations of the ψ and χ_2 rotation axes. The relative side-chain torsional entropy and side-chain heavy-atom rmsd are illustrated in panels C and D of Figure 8 for the correlated ϕ−side chain fluctuations. The occurrence of physically plausible values for both the side-chain configurational entropy and side-chain heavy-atom rmsd, which predict order parameters consistent with the observed values, demonstrate that fluctuations in a single rotamer state are sufficient to explain the experimental data.

The plots for the correlated (ϕ,ψ) fluctuations with a $c_{\phi\psi}$ value of −0.5 are qualitatively similar to those of Figure 8, with the boundary moved up 1−2° for each dihedral angle and the corresponding side-chain heavy-atom rmsd values increased approximately 0.1 Å. Hence, in this example as well, it appears that the fluctuations of the main-chain rotation axis that is gauche to the χ_2 rotation axis will be somewhat attenuated by the presence of the sterically hindered side chain.

In the relaxation analysis of ubiquitin, it was noted that the leucine methyl axis order parameter values were higher for the *pro-R* methyl in most all cases.[24] This pattern is opposite of that observed for Leu 99 of *E. coli* thioredoxin. An explanation can be found in the fact that the majority of such leucine residues in ubiquitin have mean (χ_1,χ_2) values of (−60,180), the most common leucine rotamer. Since as noted above, the two rotamers are related to each other by a pseudomirror, the calculations for the (180,60) rotamer given above apply directly to the (−60, 180) rotamer with the reversal of ϕ and ψ as well as *pro-R* and *pro-S* methyls. When the full range of physically plausible leucine side-chain fluctuations in a single rotamer state are examined, except for a few instances of high order parameters and high correlation coefficients, the methyl rotation axis having the lowest order parameter is always the one which is approximately parallel to the $C^\alpha-C^\beta$ bond vector. As a result, all main-chain fluctuations which alter the $C^\alpha-C^\beta$ bond vector orientation will likewise alter the orientation of that methyl rotation axis. In contrast, the geminal methyl rotation axis is approximately perpendicular to the $C^\alpha-C^\beta$ bond vector. Hence, main-chain fluctuations which alter the $C^\alpha-C^\beta$ bond vector orientation in the direction perpendicular to that geminal methyl rotation axis will have no relaxation effect along that axis, thus resulting in a higher order parameter for this methyl rotation axis. This analysis highlights the fact that configurational entropy estimates cannot be reliably based on the orientational distribution of the H−X bond vector alone. The geometric relationship between the H−X bond vector and the axis characteristic of the underlying conformational fluctuation must be accounted for.

It should be emphasized that only the differences in relative side-chain torsional entropy derived from eq 8 are physically meaningful. As uncorrelated leucine (σ_{χ_1},σ_{χ_2}) fluctuations of (18°,18°) predict a relative torsional entropy value of $5.8k_B$, the estimated value of $4.9k_B$ for Leu 99 corresponds to a free energy loss of 0.55 kcal/mol compared to unconstrained motion in a single rotamer state.

IVA. Conformational Entropy Arising from Rotamer State Exchange

In the effort to assess the contribution of side-chain dynamics to the entropy of protein folding, the configurational entropy of the unfolded state is commonly represented in terms of a set of disjoint multidimensional harmonic wells separated by activation barriers significantly above k_BT. In such a model, the total configurational entropy can be written as[84]

$$S_{\text{conf}} = \sum_{i=1}^{N} \omega_i S_i^{\nu} - k_B \sum_{i=1}^{N} \omega_i \ln \omega_i \qquad (10)$$

where ω_i is the probability for a given conformation and S_i^{ν} is the vibrational entropy of that state. When applied to estimating the entropy of folding, it has often been assumed that the vibrational entropy of the individual wells is the same for both the folded and unfolded states, so that the entropy change only reflects the decrease in the number of accessible conformations in the folded state. This assumption generates predictions of total entropy changes that approximate those estimated from experimental data.[85] However, for a detailed understanding of the entropy changes, variations in the individual rotamer entropies must be considered. Neglect of these effects implies the neglect of extensive correlated dynamics which are imposed by the formation of a defined tertiary structure. Conversely, since the absolute magnitude of the vibrational entropy term of eq 10 is approximately 10-fold greater than that of the conformational sampling term,[84] naive interpretation of the fixed coordinates derived from protein crystallographic analysis implies an entropy loss upon folding which would totally preclude a thermodynamically stable tertiary structure.

In a similar manner, setting $N = 1$ for the number of native conformations in the second term of eq 10 likewise misrepresents the configurational entropy of folding. On the other hand, obtaining a reliable estimate for the conformational exchange entropy term of this equation for the native state is not

(84) Karplus, M.; Ichiye, T.; Pettitt, B. M. *Biophys. J.* **1987**, *52*, 1083.
(85) Doig, A. J.; Sternberg, M. J. E. *Protein Sci.* **1995**, *4*, 2247.

straightforward. However, as illustrated below for the case of mobile solvent-exposed side chains, NMR relaxation data can provide a reasonably robust estimate of the rotamer exchange entropy of individual side chains.

The earliest NMR analyses of rotamer exchange dynamics assumed that torsion angle rotations were uncorrelated.[86] Subsequently, lattice jump models were proposed which incorporated correlated transitions.[49,87] The early assumption that small amplitude rapid (picosecond) fluctuations make a negligible contribution to macromolecular relaxation has been disproven by molecular dynamics simulations.[47] On the other hand, explicit consideration of both rotamer jumps and torsion angle fluctuations substantially increases the complexity of the model needed to fit a limited experimental data set. Some simplification can be achieved by assuming the dynamic independence of the rotamer jumps and the torsion angle fluctuations.[88]

The present study offers several advantages regarding analysis of rotamer exchange transitions. The analysis of the fast limit and generalized order parameters via an arbitrary multiexponential representation of the autocorrelation function does not assume the separability of the contributions due to rotamer jumps vs torsion angle fluctuations. Indeed, separability of the contributions due to fluctuations within disjoint multidimensional potential wells and transitions between these wells need not be generally valid for polymer dynamics.[89] The frequency partitioning provided by the S^2 and S_f^2 analysis allows for an experimental testing of separability based on the differences in time scales characteristic of the side-chain torsional fluctuations and the rotamer transitions. Furthermore, by focusing on extraction of the relevant order parameter data, estimations of the associated entropy contributions are obtained in a straightforward manner.

The 3-fold torsional potential which occurs at vicinal sp^3-sp^3 positions gives rise to a rotamer exchange conformational entropy equation of

$$S_{rot} = -k_B(p_1 \ln p_1 + p_2 \ln p_2 + p_3 \ln p_3) \qquad (11)$$

where p_i is the population of the ith rotamer. Assuming tetrahedral geometry, the order parameter arising purely from the corresponding rotamer exchange is given by

$$S^2 = 1 - {}^8/_3(p_1p_2 + p_1p_3 + p_2p_3) \qquad (12)$$

where for methyl rotation the equivalence of the rotamer populations yields the familar value of 0.111. It has been suggested that methyl groups slightly deviate from tetrahedral geometry,[90] so as to yield a limit order parameter of ~0.100.[91] The corresponding change from 8/3 to 2.7 in eq 12 has a negligible effect on the present analysis. As illustrated in Figure 9, the mapping of all possible values of $(p_1p_2 + p_1p_3 + p_2p_3)$ onto $-(p_1 \ln p_1 + p_2 \ln p_2 + p_3 \ln p_3)$ yields a reasonably narrow distribution. The upper boundary corresponds to the condition $p_1 > p_2 = p_3$. The lower left-hand boundary represents $p_1 > p_2$ with $p_3 = 0$, while the lower right-hand boundary corresponds to $p_1 = p_2 > p_3$. As explicitly verified, all other combinations of p_1, p_2, and p_3 lie within these boundaries. By utilizing the median values of this distribution, the largest possible error in the rotamer exchange entropy estimate derived from $(p_1p_2 + p_1p_3 + p_2p_3)$ is $0.08k_B$ at the $(p_1p_2 + p_1p_3 + p_2p_3)$ value of 0.25. In most cases, the anticipated error is appreciably smaller. Model studies have suggested that the quasiharmonic approximation for configurational entropy estimates of individual rotamers have errors in the range of $0.05k_B$.[71] When combined with the uncertainties in the experimental order parameter determinations, the imprecision in the mapping of experimental $(p_1p_2 + p_1p_3 + p_2p_3)$ values onto the rotamer exchange entropy estimates is unlikely to substantially affect the overall accuracy of the differential entropy calculations.

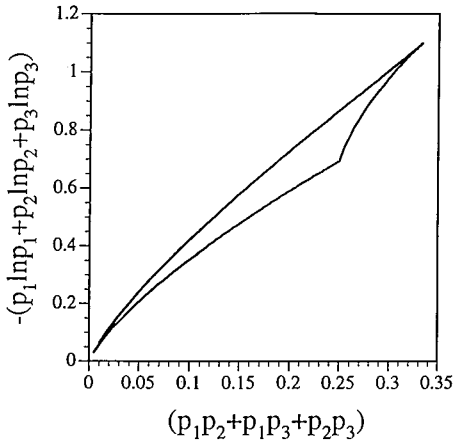

Figure 9. Torsional configurational entropy (k_B) estimated from relaxation order parameter analysis. For a 3-fold torsional potential, the order parameter for the jump process is proportional to $(p_1p_2 + p_1p_3 + p_2p_3)$. For all combinations of rotamer populations p_1, p_2, and p_3, the predicted torsional configurational entropy lies within the illustrated curve.

The foregoing analysis of conformational entropy estimates based on relaxation effects assumes that a thermodynamic quantity can be estimated from dynamical data with an upper time constant boundary of a few nanoseconds. The ergodic hypothesis ensures that the experimental data will reflect a proper population weighting of the various protein conformations. By construction, the dynamical processes analogous to the vibrational term of eq 10 lack free energy activation barriers that are large compared to thermal energy. Hence, satisfactory entropic sampling within these potential wells can be expected to occur faster than the time frame of the relaxation experiment. Furthermore, the entropic averaging for rapid configurational transitions will likewise be completed in this time frame. However, the relaxation experiment is insensitive to configurational transition terms having time constants longer than a few nanoseconds. The presence of such slow transitions implies that the corresponding order parameter would be overestimated in the experiment, resulting in a systematic underestimate of the configurational entropy. For transitions involving rotamer exchanges, the existence of entropically significant slow processes can be tested by comparison between the $(p_1p_2 + p_1p_3 + p_2p_3)$ values derived from the relaxation experiment and scalar coupling data which sample the rotamer populations in a much slower time regime.

IVB. Torsional Fluctuations and Rotamer Transitions in the Highly Solvated Side Chains of *E. coli* Thioredoxin

Operationally, the fast limit motional processes that give rise to S_f^2 can be distinguished from the slower internal motions

(86) Wallach, D. J. *J. Chem. Phys.* **1967**, *47*, 5258.
(87) London, R. E.; Avitabile, J. *J. Am. Chem. Soc.* **1977**, *99*, 7765.
(88) Batie, R. D. d. l.; Laupretre, F.; Monnerie, L. *Macromolecules* **1988**, *21*, 2045.
(89) Helfand, E. *J. Chem. Phys.* **1978**, *69*, 1010.
(90) Koetzle, T. F.; Golic, L.; Lehmann, M. S.; Verbist, J. J.; Hamilton, W. C. *J. Chem. Phys.* **1974**, *60*, 4690.
(91) Chatfield, D. C.; Szabo, A.; Brooks, B. R. *J. Am. Chem. Soc.* **1998**, *120*, 5301.

Table 1. Order Parameters and Rotamer Exchange Entropies for Solvent-Exposed Non-Hydrogen-Bonded Polar Side Chains of *E. coli* Thioredoxin

residue	$C^\alpha\ S_f^2$	$C^\alpha\ S^2$	$C^\beta\ S_f^2$	$C^\beta\ S^2$	$\sum p_i p_j$	entropy (k_B)
Asp 13	0.88	0.86	0.72	0.20	0.28	(0.88,0.94)
Lys 18	0.91	0.90	0.80	0.67	0.04	(0.18,0.21)
Glu 30	0.84	0.84	0.69	0.28	0.23	(0.65,0.81)
Glu 48	0.84	0.83	0.73	0.27	0.24	(0.67,0.83)
Gln 50	0.83	0.80	0.69	0.21	0.27	(0.85,0.92)
Gln 62	0.87	0.87	0.78	0.59	0.08	(0.29,0.35)
Lys 69	0.92	0.91	0.75	0.43	0.17	(0.52,0.64)
Asn 83	0.94	0.90	0.69	0.32	0.22	(0.64,0.79)
Lys 100	0.84	0.80	0.71	0.36	0.18	(0.56,0.68)
Glu 101	0.88	0.86	0.72	0.26	0.25	(0.69,0.86)

which contribute to additional observed relaxation effects. Perhaps the simplest nontrivial case of interpreting these relaxation effects in terms of specific motional models is that of the highly solvated side chains. In Table 1 are listed the C^α and C^β order parameters of the 10 polar *E. coli* thioredoxin side chains for which the C^α S^2 is greater than 0.8, the C^β atoms have solvent accessible surface areas of greater than 5 Å^2, and there are no side-chain−main-chain (direct or water-mediated) hydrogen bonds as reported in the X-ray analysis.[36] It should be noted that the NMR relaxation studies and the X-ray structural analysis were carried out under quite similar pH and ionic strength conditions, and an excellent correspondence between surface side-chain hydrogen bonding and elevated order parameters has been previously reported.[4] The similarity of the C^α S^2 and S_f^2 values in Table 1 indicates no significant internal rotational reorientation dynamics of these main-chain positions in the time frame of the Larmor frequencies. As a result, it is concluded that the marked decrease in the C^β S^2 values as compared to the corresponding S_f^2 values observed for most of these side chains can be analyzed in terms of the local side-chain dynamics.

For each of these 10 side chains, the predicted dominant time constant is substantially longer than that of the high-frequency partition boundary $4\omega_{H+C}$. This result indicates the plausibility of interpreting S_f^2 in terms of fluctuations within a rotamer well and interpreting ($S_f^2 - S^2$) in terms of transitions between rotamer wells. If the fluctuations within a rotamer well are unimpeded by additional intramolecular interactions, the local torsional potential should impose an approximately Gaussian torsional fluctuation with an rmsd of near 18°.

In the analysis of the buried side-chain dynamics described above, the predicted order parameters were examined as a function of the main-chain and side-chain fluctuations and correlation coefficients. Despite the recognition that restricted side-chain motion provides the basis for the correlated torsional fluctuations, the side-chain heavy-atom rmsd values arose as a prediction rather than as an input parameter to the optimization. In an analogous fashion, the magnitude of the χ_1 fluctuations of the solvent-exposed non-hydrogen-bonded polar side chains can be viewed as a predicted parameter, with the expectation that the optimal value should reflect the local torsional potential.

For the 10 mobile side chains of Table 1, the predicted χ^2 fit to the C^α and C^β order parameters as a function of the torsional fluctuations σ_{χ_1} and the main-chain−side-chain correlation coefficients are illustrated in Figure 10. For each value of σ_{χ_1} and correlation coefficients, the values of σ_ϕ and σ_ψ (assumed to be equal) were varied independently for each side chain so as to obtain the minimum χ^2 residual summed over the population of the 10 residues. In all cases, the predicted optimal σ_{χ_1} value is rather precisely determined. When no main-chain or side-chain correlation is assumed, the fit is poor, and the σ_{χ_1} optimum is smaller than expected. As the solvent interactions can be expected to impose a dynamic drag on the torsional fluctuations of the C^γ atoms, the effects of correlation were examined for χ_1 and the main-chain rotation axis, forming a crankshaft orientation relative to the C^β−C^γ bond. Although the effects of this correlation on the predicted χ^2 residuals are modest, the σ_{χ_1} optimum is highly sensitive to this correlation.

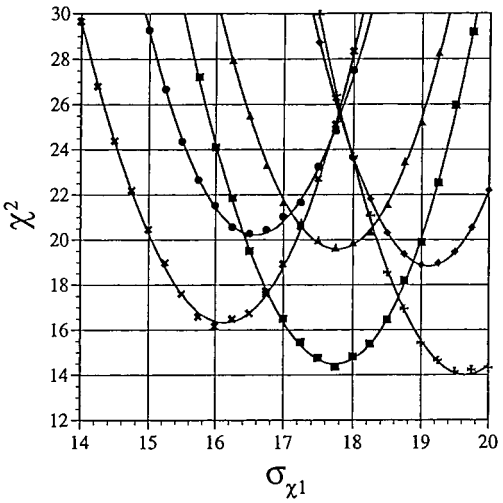

Figure 10. Prediction of the C^α and C^β S_f^2 values for the solvent-exposed side chains of Table 1 as a function of χ_1 and mainchain torsional fluctuations ($\sigma_\phi = \sigma_\psi$) and correlation coefficients. For a fixed set of σ_{χ_1} and correlation coefficients, the main-chain torsional fluctuations were adjusted for each residue so as to minimize the aggregate χ^2 residual summed over the 10 residues. Assuming no torsional correlation (●) yields the highest χ^2 residual. Introduction of weak (0.25 (▲)) and modest (0.50 (◆)) main-chain−χ_1 correlations has little effect on the χ^2 residual but substantially increases the σ_{χ_1} optimum. Introduction of main-chain ϕ−ψ correlation (−0.5 (×)) significantly decreases the χ^2 residual but shifts the σ_{χ_1} optimum away from the expected 18°. The combination of modest main-chain ϕ−ψ correlation (−0.5) and weak main-chain−χ_1 correlation (0.25) (■), consistent with reported correlation coefficients derived from molecular dynamics[74,75] provides a favorable combination of a lower χ^2 residual near the expected σ_{χ_1} optimum.

Quite the opposite effect arises from the assumption of main-chain (ϕ,ψ) correlation. A modest level of (ϕ,ψ) correlation (i.e., −0.5) significantly decreases the predicted χ^2 residual but shifts the χ_1 optimum to a smaller angle. When a $c_{\phi,\psi}$ of −0.5 is combined with a weak main-chain−χ_1 correlation (i.e., 0.25), both the χ^2 residuals and the σ_{χ_1} optimum are substantially superior to those predicted from the uncorrelated fluctuations. It should be noted that both of these correlation coefficients match well with those estimated from molecular dynamics simulations.[74,75] Since Glu 62 and Asn 83 contributed substantially to the χ^2 residual calculations, the calculations were repeated with those residues removed. The correlation dependence of the χ^2 residuals was unchanged, and in no case did the predicted σ_{χ_1} optimum differ from that of Figure 10 by more than 0.25°.

For half of the C^β values listed in Table 1, the relaxation data for both $^1H^\beta$−$^{13}C^\beta$ vectors were obtained, and the order parameter predictions of Figure 10 utilized all 15 individual values. However, in no case did the geminal order parameters differ by more than the average estimated accuracy of 0.034 (the combination of both experimental and multiexponential analysis model precision). The similarity of the observed geminal order parameters, which was previously noted to be common throughout the protein structure,[4] provides additional insight into the presence of correlated motion.

Torsional fluctuations around the main-chain rotation axis parallel to the $C^{\beta}-C^{\gamma}$ bond can have no differential effect on the geminal $^1H^{\beta}-^{13}C^{\beta}$ order parameters. Correlation between this main-chain fluctuation and χ_1 fluctuation does not alter the absence of a differential effect. In contrast, torsional fluctuations about the other main-chain rotation axis can have a marked differential effect, as the $^1H^{\beta}-^{13}C^{\beta}$ bond vector parallel to this main-chain rotation axis is largely insensitive to its torsional fluctuations. However, the near equivalence of the $^1H^{\beta}-^{13}C^{\beta}$ order parameters can be achieved by only modest correlation between fluctuations of this main-chain torsional angle and χ_1. For a σ_{χ_1} value of 18° and a C^{α} S^2 value of 0.85, uncorrelated (ϕ,ψ,χ_1) fluctuations predict a differential $^1H^{\beta}-^{13}C^{\beta}$ order parameter of 0.059. Introduction of crankshaft-like correlations decreases this difference only modestly. A $c_{\phi,\psi}$ value of -0.5 decreases the differential $^1H^{\beta}-^{13}C^{\beta}$ order parameter to 0.038, while combination of this (ϕ,ψ) correlation with a modest main-chain$-\chi_1$ correlation of 0.25 further decreases the predicted differential $^1H^{\beta}-^{13}C^{\beta}$ order parameter to 0.023, below the level reliably detected with the quality of the present relaxation data. It should be noted that Kay and co-workers have reported that a modest fraction of the side-chain methylene positions of the N-terminal SH3 domain of drk do exhibit nonequivalence in the geminal order parameters.[6]

The foregoing analysis suggests that the assumption of independent main-chain and side-chain fluctuations may be unfounded, even in the case where interresidue interactions are not directly imposing correlated motion. Furthermore, this analysis supports the plausibility of interpreting the C^{β} S_f^2 values of the highly solvated non-hydrogen-bonded side chains in terms of torsional fluctuations within a given rotamer state. As discussed in section IIIA, evidence that transitions between χ_1 rotamer wells generally do not significantly contribute to the estimated C^{β} S_f^2 values is drawn from the lower bound of the order parameters estimated from fluctuations within a single rotamer state. Assuming the optimum from Figure 10 for the case of a $c_{\phi,\psi}$ of -0.5 and a main-chain$-\chi_1$ correlation of 0.25, for a C^{α} S^2 of 0.80, the predicted C^{β} S^2 is 0.68, which is within experimental error of the lowest experimental non-proline, nonterminal C^{β} S_f^2 value. Extending this analysis to the χ_2 dihedral angle, superimposing an 18° Gaussian fluctuation of χ_2 upon the same set of single rotamer main-chain and side-chain fluctuations predicts a C^{γ} S^2 value of 0.52 for a C^{α} S^2 value of 0.80. This compares quite favorably with the lowest non-proline C_{γ} S_f^2 value of 0.50 in the protein.

The suggestion that, in general, methine and methylene S_f^2 values do not manifest the dynamics of rotamer transitions gains further plausibility from the data of Figure 2. Although these experimental data quite effectively fill much of the contour which defines the range of relaxation values consistent with an arbitrary multiexponential autocorrelation function, the lower right-hand region is notably empty. This region represents motions with amplitudes larger than fluctuations in a single rotamer well with apparent time constants that are rapid compared to $1/\omega_{H+C}$. In fact, the relaxation data for the majority of the methyl resonances lie within this blank region of Figure 2, thus demonstrating that the full range of the multiexponential autocorrelation function contour is physically accessible. In contrast to the methyl rotation dynamics, for which transition times of ~50 ps are predicted,[65] side-chain rotamer transitions in proteins involving heavy-atom movement are significantly slower.

For the 10 solvent-exposed residues listed in Table 1, the C^{β} S_f^2 values appear explicable in terms of correlated fluctuations within a rotamer well. Given that only fast limit motion is apparent for the corresponding C^{α} positions, the C^{β} S^2 values should be explicable in terms of rotamer exchange transitions. In the case of arbitrarily narrow rotamer wells, the order parameter for the rotamer transitions is proportional to $(p_1p_2 + p_1p_3 + p_2p_3)$. For the two- and three-rotamer jump conditions defining the boundary limits of Figure 9, it was explicitly verified that transitions between rotamer wells with widths of 18° rmsd likewise predict an order parameter which depends only on $(p_1p_2 + p_1p_3 + p_2p_3)$. Furthermore, it is found that, to a good approximation the C^{β} (S^2/S_f^2) value provides a reliable estimate for determining $(p_1p_2 + p_1p_3 + p_2p_3)$ from eq 12, although due to the collinearity of the fast limit and rotamer transition rotation axes this relationship cannot be rigorously correct.

In Table 1 are listed the $(p_1p_2 + p_1p_3 + p_2p_3)$ values determined for each of the 10 residues along with the corresponding extrema values for the rotamer exchange entropies as derived in Figure 9. The maximum range of entropy values ($0.17k_B$ for Glu 101) corresponds to less than 0.1 kcal/mol in free energy at room temperature. The range of possible rotamer exchange entropy values can be further reduced by considering independent information on rotamer populations derived from scalar coupling analysis or from measurement of dipole−dipole cross correlation effects.[38,92] When differential torsional entropy comparisons are made to the totally unhindered rotamer exchange, as might be assumed for the unfolded state of a protein, the reference $(p_1p_2 + p_1p_3 + p_2p_3)$ value will not be 1/3 as predicted for equal rotamer populations. Typical estimations of the χ_1 rotamer populations of (0.50,0.35,0.15) for χ_1 values of (−60°,180°,60°) yield a $(p_1p_2 + p_1p_3 + p_2p_3)$ value of 0.30.

The capability of estimating the torsional entropy arising from fluctuations in a rotamer well combined with the capability of estimating the entropy arising from rotamer exchange transitions indicates that it should be increasingly feasible to experimentally ascertain the net contribution of side-chain immobilization to the overall entropy of protein folding.

V. Conclusions

Using a multiexponential autocorrelation function representation for estimation of S^2 and S_f^2, the present analysis demonstrates the utility of relaxation data in determining correlated side-chain fluctuations and the resultant torsional configurational entropy effects. The analysis suggests that, for the case of large buried side chains, the correlated main-chain−side-chain torsional fluctuations results in the attenuation of the main-chain torsional fluctuations gauche to the $C^{\beta}-C^{\gamma}$ bond. Furthermore, low order parameters for leucine methyl rotation axes can be consistent with fluctuations within a single rotamer state. The marked difference between the order parameters of geminal leucine methyl rotation axes demonstrates the necessity of considering distal torsion angle fluctuations. Analogous considerations have motivated the analysis of internal restricted correlated rotations reported by Daragan and Mayo,[74,92] although their recent analysis of protein side-chain dynamics,[93] which assumes that distal side-chain atoms do not influence the motions of H−C bonds closer to the backbone, is inconsistent with the conclusions of the present study.

The configurational entropy of motionally restricted positions cannot be satisfactorily rationalized using local H−X bond

(92) Daragan, V. A.; Mayo, K. H. *Prog. Nucl. Magn. Reson. Spectrosc.* **1997**, *31*, 63.
(93) Daragan, V. A.; Mayo, K. H. *J. Magn. Reson.* **1998**, *130*, 329.

reorientation models. Attempts to estimate configurational entropy using local H−X bond reorientation models have arisen primarily as a result of the sparseness of the monitored sites for the majority of protein relaxation studies. The demonstration of substantial correlation of torsional fluctuations presented herein clearly indicates that reliable experimental estimates of configurational entropies necessitate a more extensive dynamical mapping of the relaxation behavior throughout the protein structure, as offered by the alternate carbon enrichment approach used here.[4] ^{2}H relaxation autocorrelation analysis[3,6] and/or dipole−dipole cross correlation studies[6,38,92] will likely prove to be of considerable use in analysis of correlated protein side-chain dynamics, although the inability to obtain frequency partitioning of the order parameter contributions via these experiments may represent a significant limitation in practice.

The success in rationalizing a significant fraction of the observed relaxation data in terms of comparatively localized torsional motion should not be construed as an argument for only such modes of motion being present in the protein molecule. In particular, finding predicted side-chain heavy-atom rmsd values consistent with X-ray Debye−Waller factors does not imply that the local torsional motion constitutes the total atom mobilities. As demonstrated in early molecular dynamics simulations of cytochrome *c*,[94] superimposed on the more rapid torsional oscillations are often slower concerted motions which, on the length scale of the residue, appear primarily as translational disorder. Pure internal translational motion is transparent to these relaxation experiments. Segmental translations appear to account for a substantial fraction of the nonharmonic components of protein dynamics.[95] For most of the H−X bond vectors involved in such segmental transitions, the relaxation effects are likely negligible. However, the shifts in the relative orientation for the α-helices of myoglobin seen by molecular dynamics simulations were accompanied by side-chain rearrangements so as to preserve the close packing of the protein interior.[95] If NMR relaxation analysis is to effectively quantitate contributions from such larger scale cooperative transitions, it will be essential to first optimize the ability to quantitate the relaxation contributions from the generally more rapid localized dynamics. It is anticipated that the capability of determining both the fast limit and generalized order parameters will prove critical for reliably distinguishing the relaxation contributions from localized vs larger scale cooperative motions.

Despite the wide range of conformational dynamics which can be represented in terms of a multiexponential autocorrelation function, the range of relaxation parameters consistent with such an autocorrelation function is clearly delineated. Experimental data which fall significantly outside of these bounds, which cannot be explained by chemical exchange broadening unambiguously indicate a failure of either the data collection or the dynamics analysis. As the described order parameter analysis depends on only the operational separability of the relaxation due to global tumbling and the validity of the multiexponential autocorrelation function as embodied in eq 7, it comes rather close to deserving the appellation “model-free”.

Acknowledgment. Clifford Unkefer and James Brainard are gratefully acknowledged for stimulating discussions. This work was supported in part by NIH Grant GM38779.

JA982988R

(94) Morgan, J. D.; McCammon, J. A.; Northrup, S. H. *Biopolymers* **1983**, *22*, 1579.

(95) Elber, R.; Karplus, M. *Science* **1987**, *235*, 318.